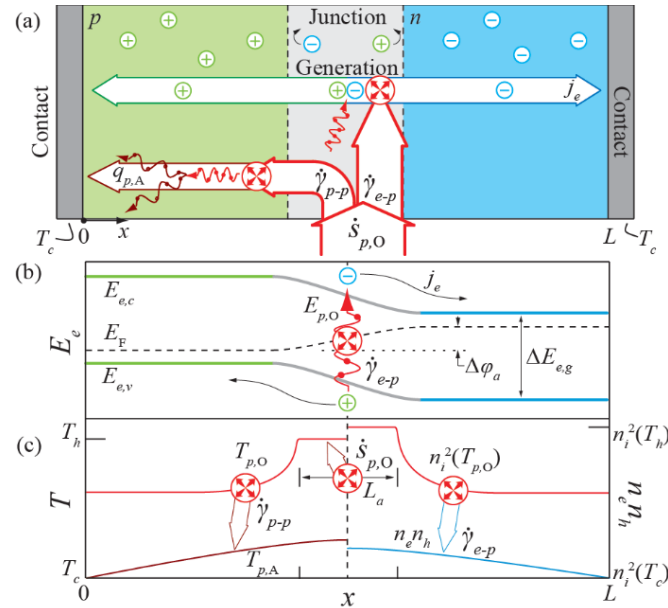


Resonant phonon harvesting



Massoud Kaviani

Department of Mechanical Engineering

Heat Transfer Physics Group

University of Michigan

University of Tokyo, January 20, 2017



Abstract

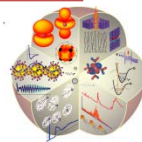
Through multiscale analyses we introduce harvesting of resonant optical phonons in semiconductors, with three new concepts:

- *phonon recycling* (absorption) in in *graded heterojunction* for partial reversal of the joule heating,
- *phonovoltaic* for direct hot-phonon-energy conversion, and
- *phonocatalysis* with phonon-controlled chemisorbed dissociation.

In reversing the joule heating through in-situ phonon recycling (pR), we tune a heterojunction barrier height to optical phonons and optimize it for GaAs:Al electron channel for maximum phonon absorption. We calculate the pR efficiency of this partial reversal of phonon emission.

In phonovoltaic (pV) with nonequilibrium optical phonon source and phonon generation of charge pairs in *p-n* junction to generate power, we define the pV figure of merit and explore the optimal material for efficient room-temperature pV. We search for pV materials and tune the graphene composite h-C:BN bandgap to its C=C bond optical phonons and evaluate the pV efficiency.

In phonocatalysis (pC) with *ab initio* molecular dynamics we show the chemisorbed dissociation of XeF₆ on h-BN surface leads to formation of XeF₄ and two surface F/h-BN bonds. We show that the chemisorbed dissociation (the pathway activation ascent) requires absorption of large-energy optical phonons. Then using progressively heavier isotopes of B and N atoms, we show that limiting these high-energy optical phonons inhibits the chemisorbed dissociation, i.e., controllable pC..



Outline

1. Hot Optical Phonons in Energy Conversion
2. Phonon Recycling Heterobarrier (*PRB*, **95**:85301, 2015)
3. Phonovoltaic (*PRB*, **93**:094302 and 125203, and **94**:245412 , 2016)
4. Phonocatalysis (*AIP Advances*, **6**:065124, 2016)
5. Conclusions and Outlook

Acknowledgment



1. HOT OPTICAL PHONONS IN ENERGY CONVERSION

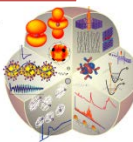
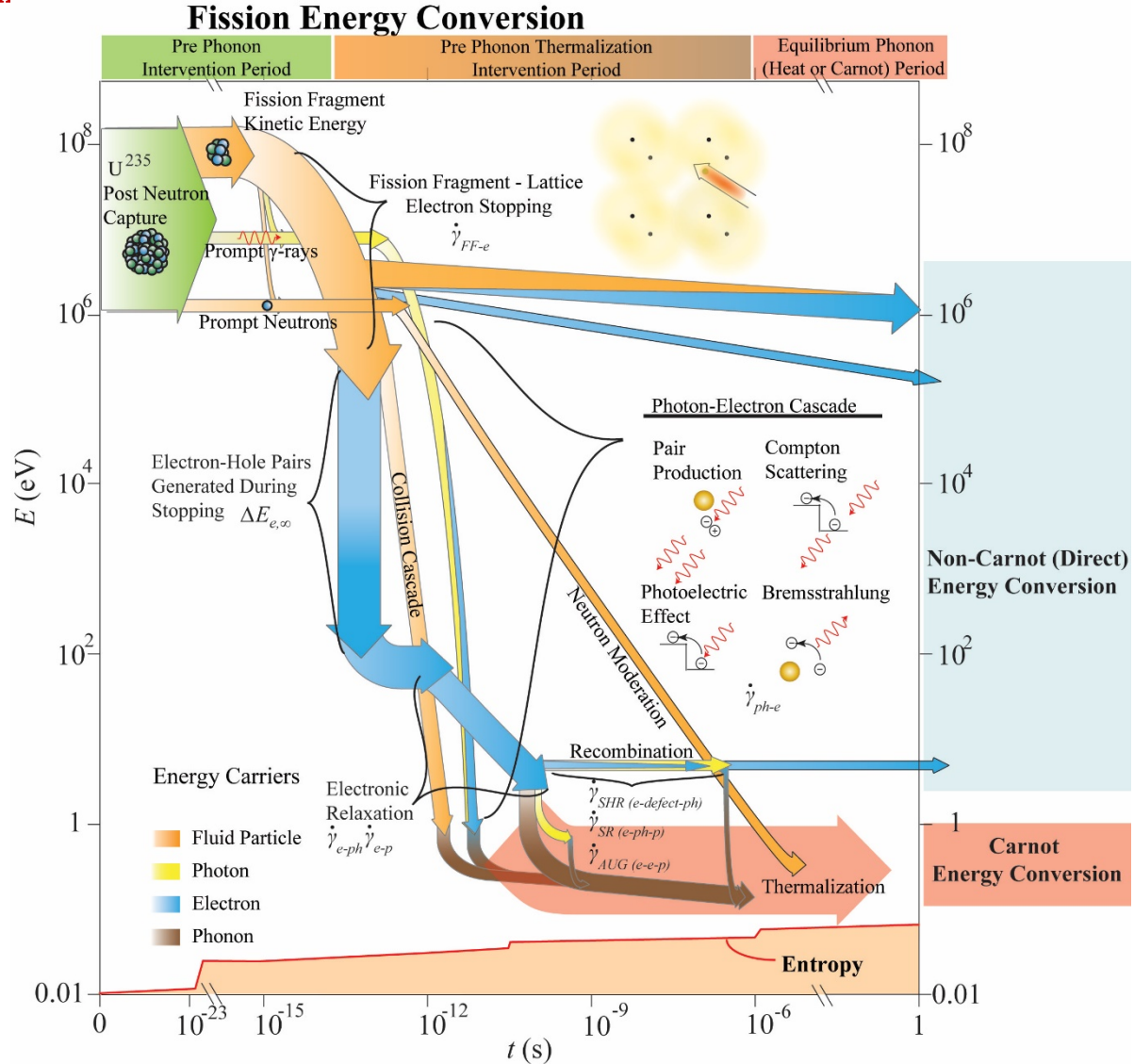
Nuclear energy-time diagram

When a fissionable nucleus captures a neutron, its energy increases dramatically due to, neutron pairing, mass decrease, and neutron energy (for fast neutrons)

Nucleus begins to deform until the coulomb force overcomes the strong force.

Nucleus scissions, creating ~ 200 MeV in the form of: two energetic fission fragments (~ 170 MeV total), γ -rays (~7 MeV), and fast neutrons (~ 5 MeV)

The figure to right shows the path of the fission energy over time, the causes for its quality loss, and some direct energy conversion pathways .

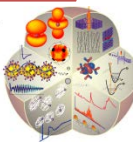
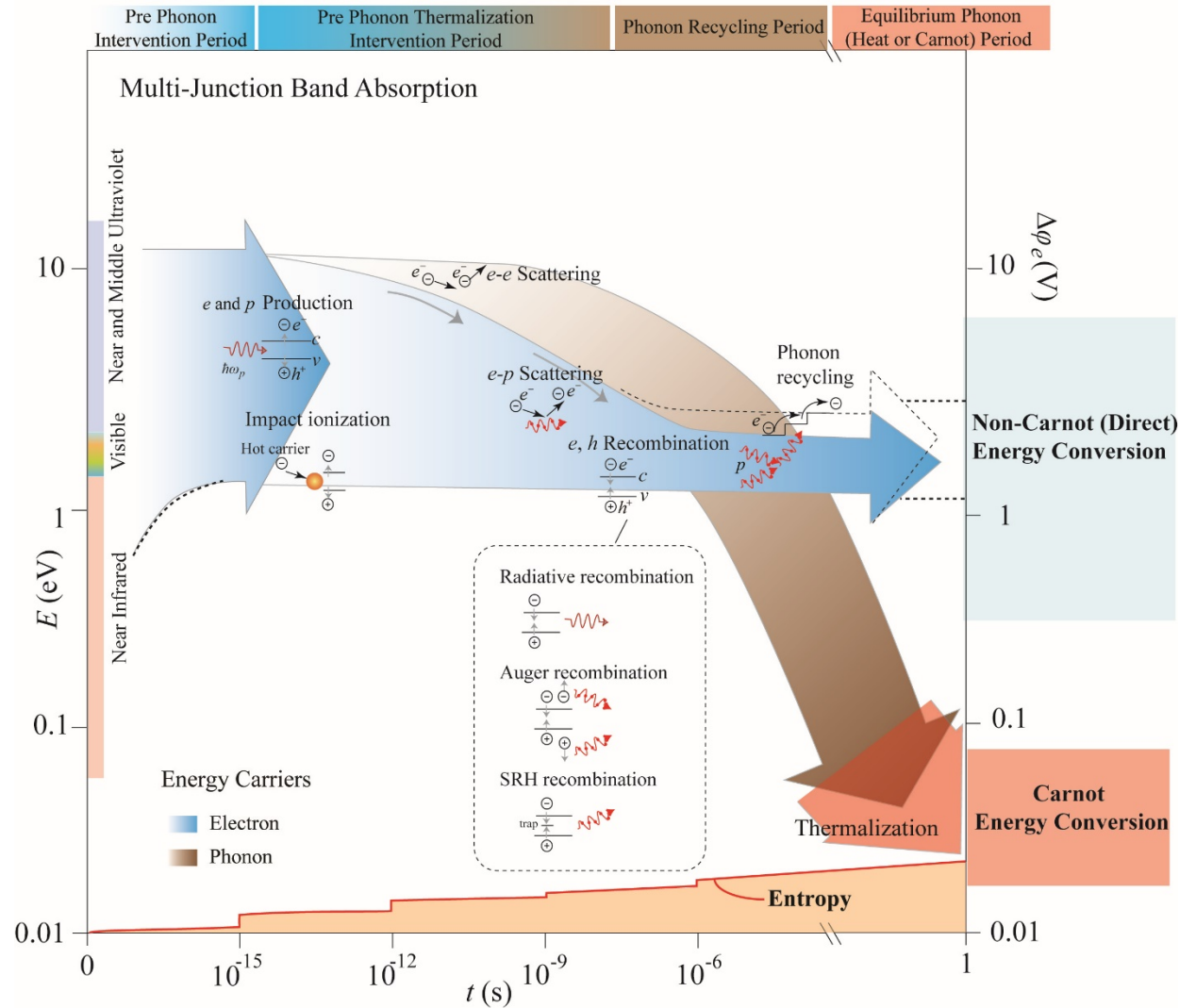


Solar photovoltaic energy-time diagram

Solar Energy Conversion

Figure to right shows the energy-time evolution of solar energy in photovoltaic conversion. Phonons are emitted by decay of hot electrons, by electron-hole recombination, and by decay of intraband excited electrons.

These phonons may be recycled through a heterogeneous barrier transition, where they gain electric potential.



Chemical-bond energy-time diagram

Chemisorbed Energy Conversion

Can we directly convert chemical energy to electrical energy?

Main processes:

Chemical-bond energy

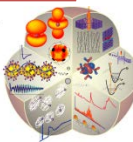
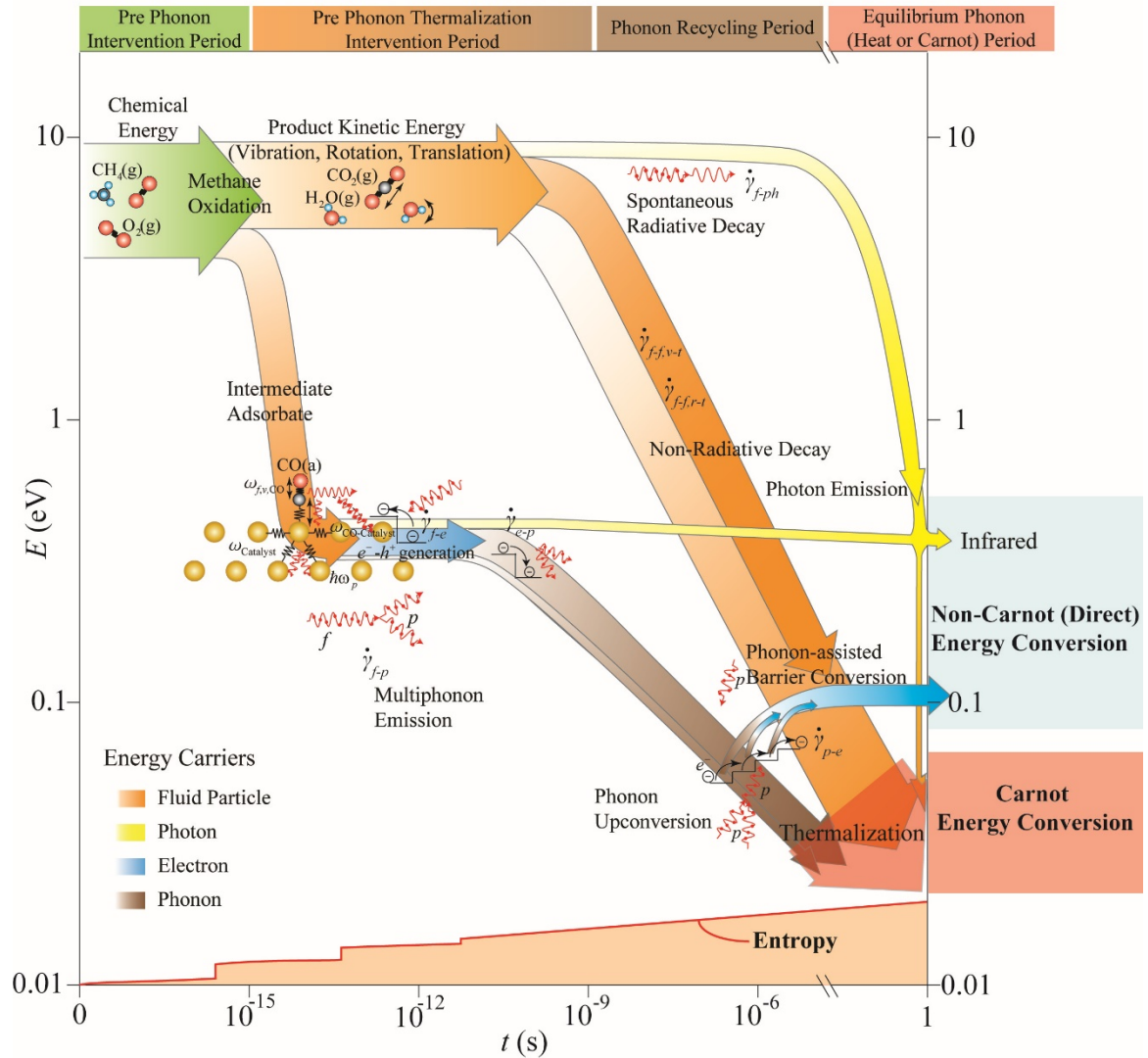
-> kinetic energy of fluid particles

Kinetic energy (chemisorption)

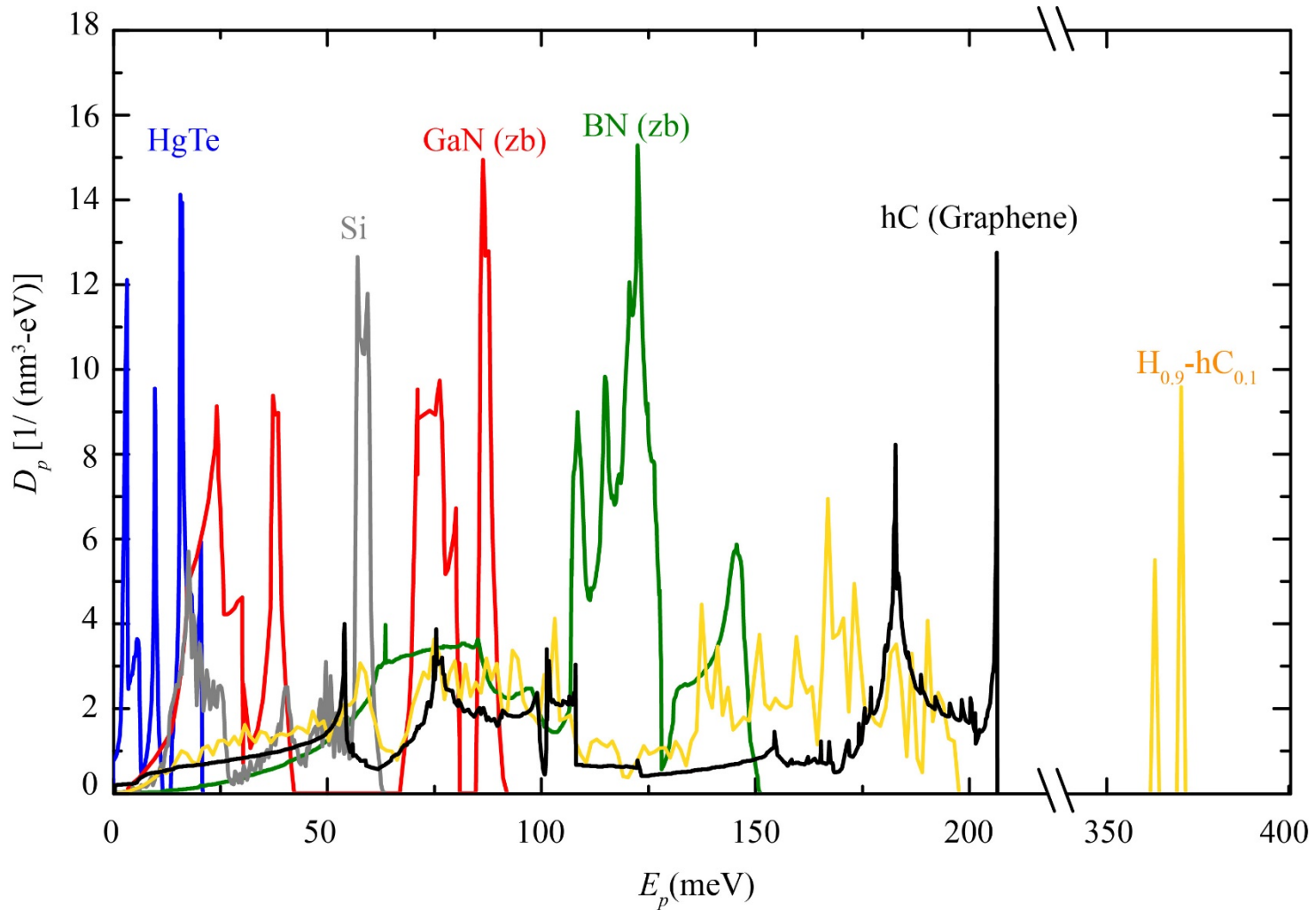
-> phonons in solid

Phonons

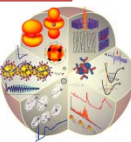
-> potential energy of circuit electrons



Resonant Phonon in Semiconductors (Graphene is Metallic)

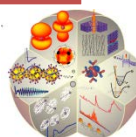
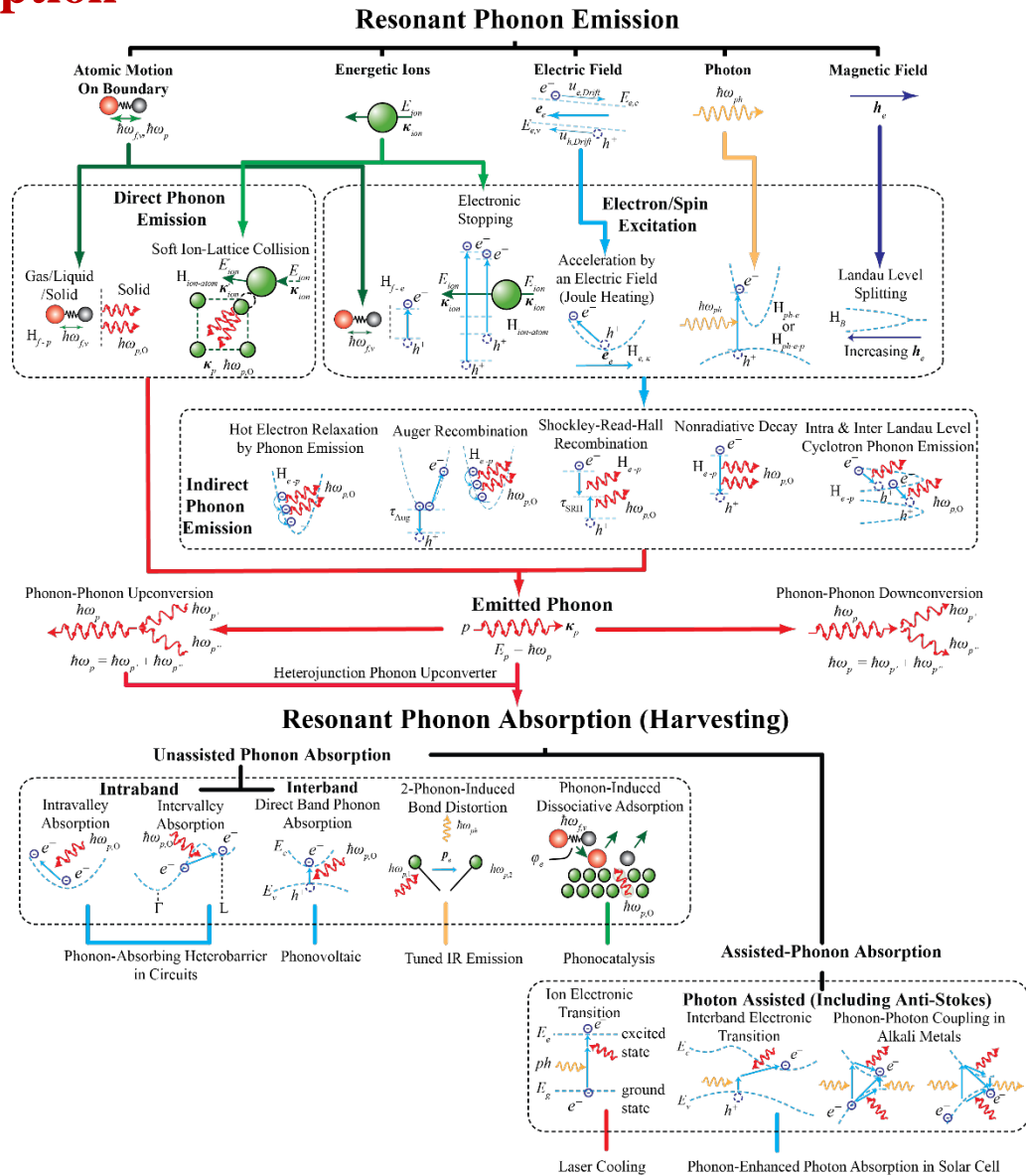


Note the high energy optical phonon of hydrogenated graphene (a semiconductor) is due to the H-C bond.



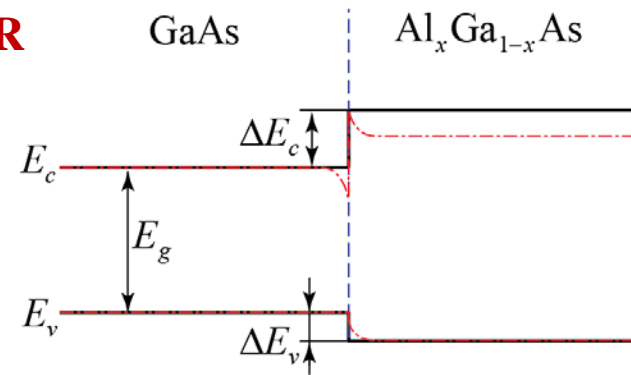
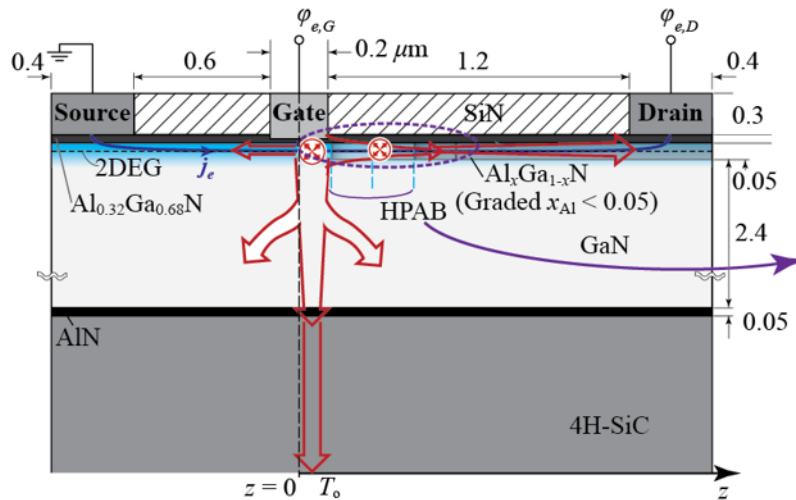
Phonon emission and absorption

While phonon emission occurs in all energy conversions in solids (part of increase in entropy), phonon absorption requires special conditions and designs.



2. PHONON RECYCLING HETEROBARRIER

We propose the **potential barrier structure** for phonon energy conversion back to electron.



- Heterobarrier structure composed of **GaAs** and $\text{Al}_x\text{Ga}_{1-x}\text{As}$ (x or x_{Al} is the Al content)
- $E_{g,\text{Al}_x\text{Ga}_{1-x}\text{As}} > E_{g,\text{GaAs}}$ ($\text{Al}_x\text{Ga}_{1-x}\text{As}$: $E_g = 1.424 + 1.247x$ eV)
(Thus, interface has a band edge discontinuity in the conduction ΔE_c and valence bands ΔE_v depending on x_{Al}).

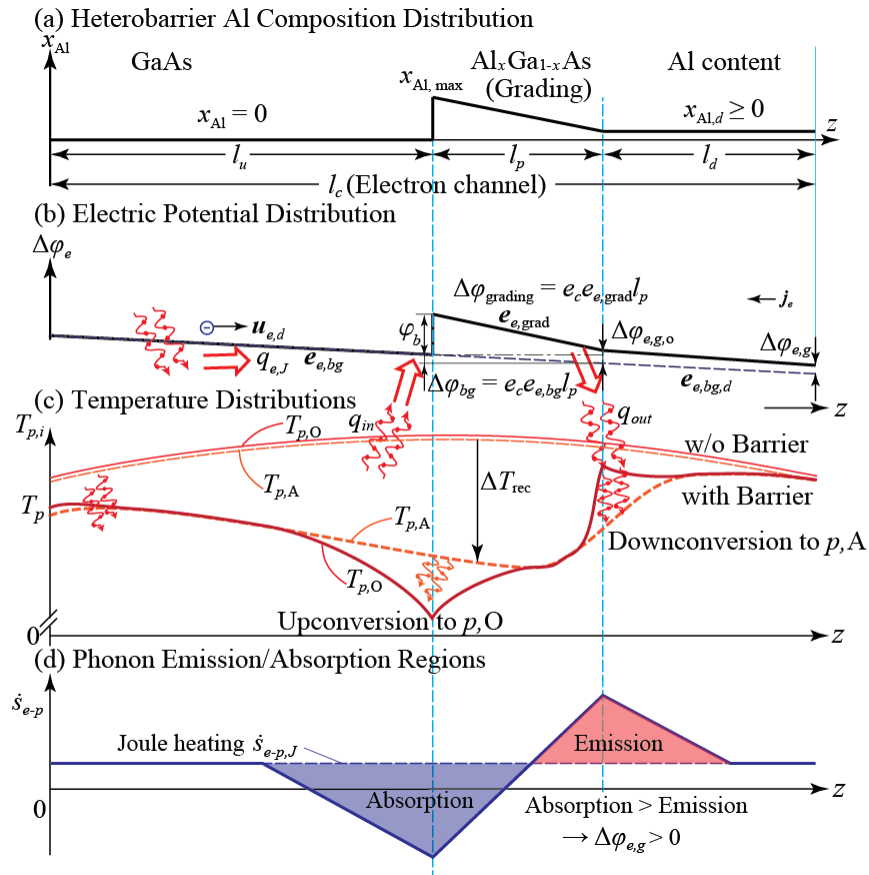
$$\Delta E_c = 0.79x \text{ eV}, x < 0.41 \text{ and } \Delta E_v = -0.46x \text{ eV}.$$

- With electrons as the main charge carriers, conduction band edge discontinuity ΔE_c is regarded as a barrier, and the barrier height ϕ_b can be controlled with x_{Al} .

Ideal band discontinuity of GaAs/ $\text{Al}_x\text{Ga}_{1-x}\text{As}$.



Phonon Absorbing Barrier (PAB) Structure



Phonon absorption barrier (PAB)

- Energy conversion into electric potential using the barrier structure
- Potential barriers can cause an **adverse (or reverse) current** by reflection or potential change
 → To compensate this adverse effect, large, forward local electric field formed by x_{Al} grading ($e_{e,HPAB}$) is introduced in the barrier.
- Phonon absorption populates electrons with $E_e > \phi_b$ before or after the barrier transition, and this energy is converted to electric potential.

Spatial distributions of x_{Al} , electric field and potential, and optical and acoustic phonon temperatures in the phonon absorbing barrier structure (PAB). x_{Al} is abruptly increased to create the potential barrier ϕ_b in the conduction band edge, while the grading maintains the current.



Interaction kinetics in semiconductors

• Optical phonon interaction rate

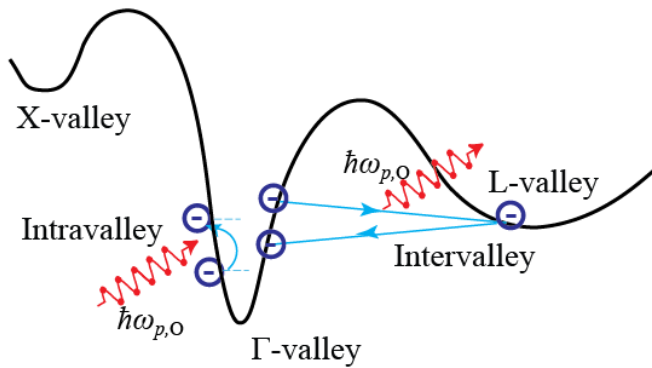
Considering perturbation by the displacement $d = [\hbar/(2m\omega_{p,O})]^{1/2}(b^\dagger + b)$

$$H = H_0 + H_{e-p} = (H_{e,o} + H_{p,o}) + \phi'_{e-p}d,$$

$$\dot{\gamma}_{e-p,O} = \frac{\pi}{m\omega_{p,O}} \left| \langle \psi_{e,f} | \phi'_{e-p} | \psi_{e,i} \rangle \right|^2 \left| \langle f_p \pm 1 | b^\dagger + b | f_p \rangle \right|^2 \delta_D(E_{e,f} - E_{e,i} \mp E_{p,O}).$$

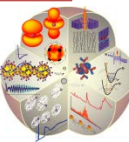
$$\left| \langle \psi_{e,f} | \phi'_{e-p} | \psi_{e,i} \rangle \right|^2 = \begin{cases} \text{isotropic nonpolar optical phonon} & \phi_{e-p}'^2 \delta_{D,\kappa} \\ \text{anisotropic polar optical phonon} & \frac{\rho e_c^2 \omega_p^2}{\kappa_p^2} \left(\frac{1}{\epsilon_\infty} - \frac{1}{\epsilon_s} \right) \delta_{D,\kappa} \end{cases}$$

$$|\langle f_p \pm 1 | b^\dagger + b | f_p \rangle|^2 = f_p + 0.5 \pm 0.5$$



In **GaAs**, the following optical phonon interactions are considered for energy conversion

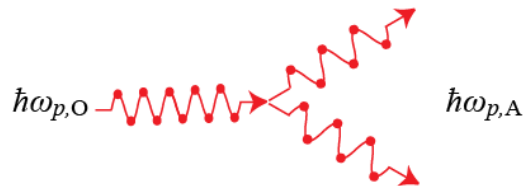
- **Intravalley Polar Optical** (GaAs – Polar, LO phonon)
- **Intravalley Nonpolar Optical**
- **Intervalley Optical**



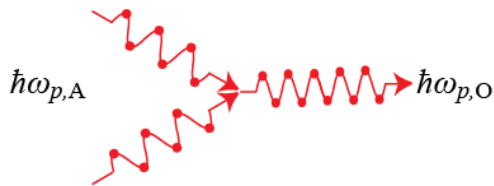
Phonon-phonon interactions

- Hot phonons are also decayed by downconversion to acoustic phonons (competing with e - p interaction).
- Optical phonon scattering by three-phonon interactions (up- and downconversion) [1]

Optical-Acoustic Downconversion



Acoustic-Optical Upconversion



$$\dot{\gamma}_{p-p} = \frac{\hbar}{8\pi\rho^3} \frac{|M_{p-p}|^2 R}{u_{p,A}^7 u_{p,O}^2} \omega_{p,A}^2 \omega_{p,O}^3 (f_{p,A} + \frac{1}{2} \pm \frac{1}{2})(f_{p,A} + \frac{1}{2} \pm \frac{1}{2})(f_{p,O} + \frac{1}{2} \mp \frac{1}{2})$$

At 300 K

$$\dot{\gamma}_{p-p,dn} = 2.34 \times 10^{11} \text{ s}^{-1} \quad (\tau_{p-p,dn} = 4.27 \text{ ps})$$

$$(\gamma_G = 0.8, R = 0.128, u_{p,A} = 2800 \text{ m/s for GaAs})$$

From other literatures [2-6], $\tau_p = 2 \sim 9$ ps (As the optical phonon population increases, the down-conversion rate increases)

$\dot{\gamma}_{p-p} < \dot{\gamma}_{e-p}$: the e - p interaction rate is faster than the p - p

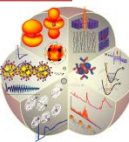
(Thus, during the hot-phonon relaxation, electrons are first excited and relaxed to equilibrium.)

Hot phonon - small average speed and downconversion to acoustic phonons

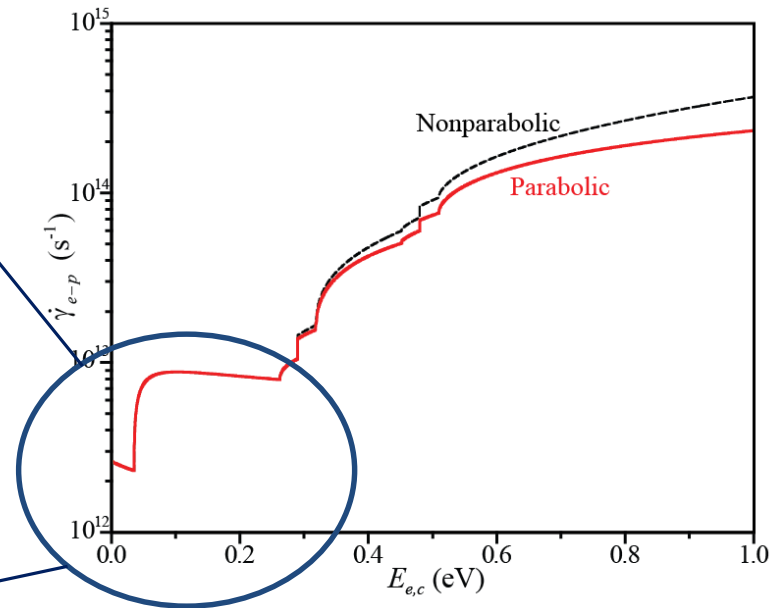
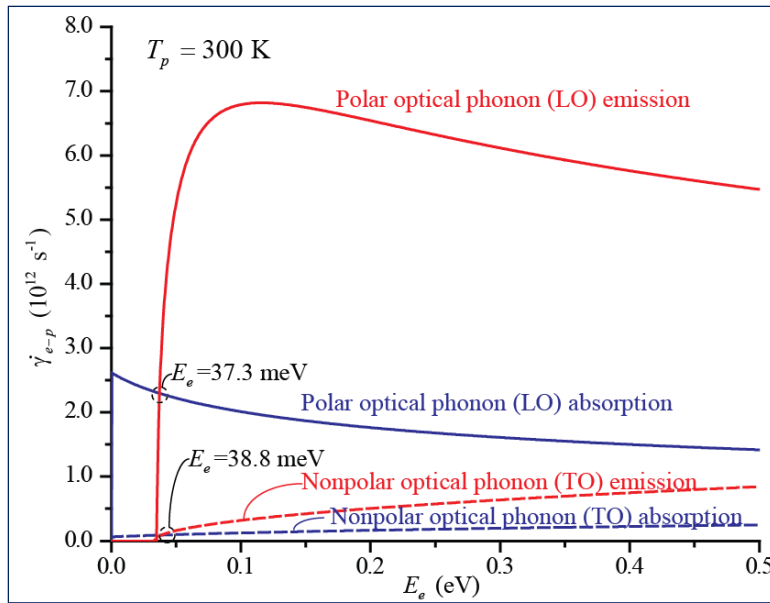
→ The hot phonons should be used **quickly and close to their emission site.**

[1] J. Singh, *Electronic and Optoelectronic Properties of Semiconductor Structures*, Cambridge (2003).

[2] J. A. Kash, Proc. SPIE **942**, 138 (1988). [3] APL **97**, 033110 (2010) [4] APL **80**, 4303 (2002) [5] PRL **44** 1505 (1980) [6] PRB **30** 4501 (1984)



Electron-optical phonon interaction



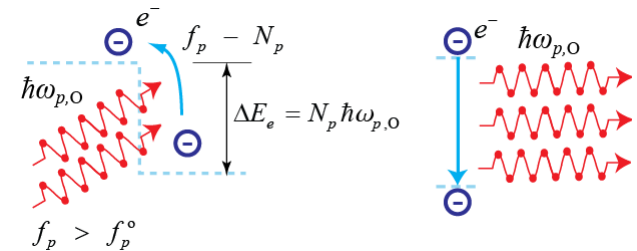
• Polar optical phonon scattering in Γ valley is dominant at low electron energy [1-3].

• **Multiphonon interaction** – electron simultaneously absorbs or emits multiple phonons. [4]

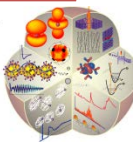
1) First-order time-dependent perturbation theory / High-order coupling

2) High-order perturbation/ Linear coupling (φ_{e-p})

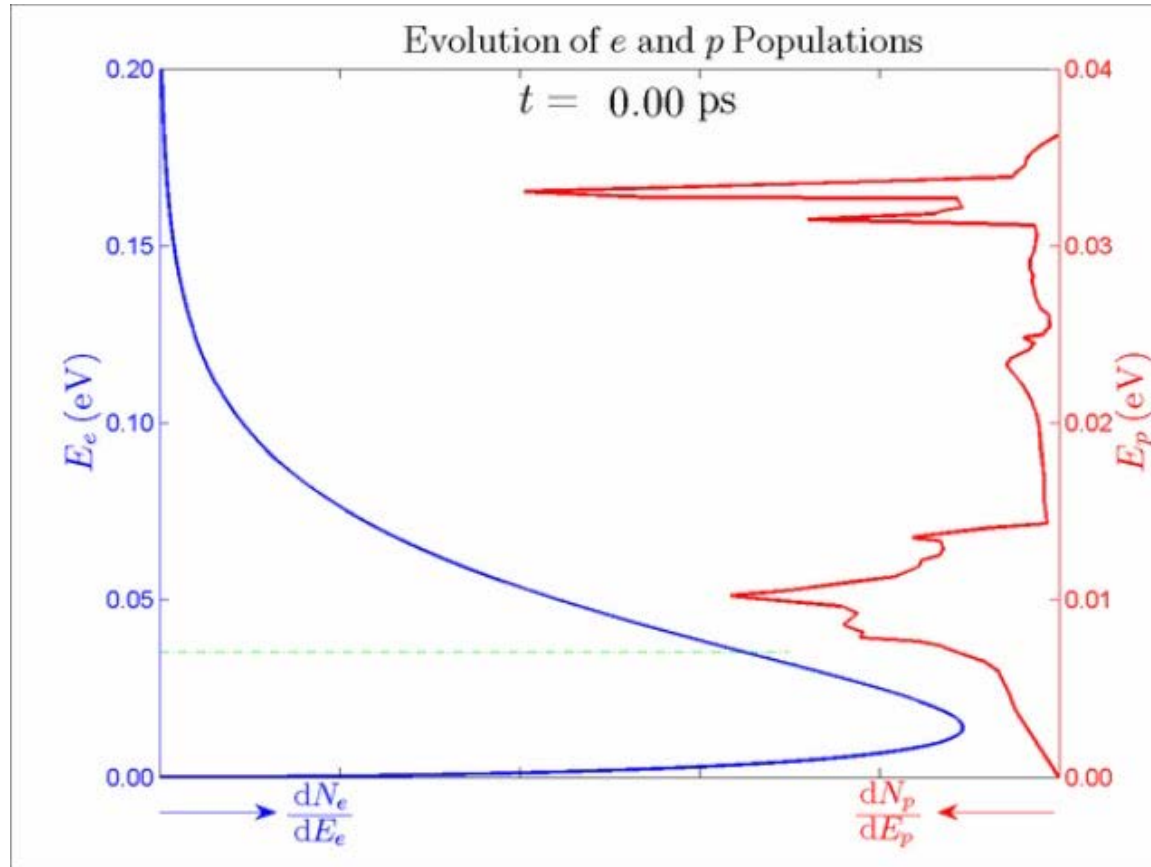
=> Not probable: small interaction rate, high phonon population for absorption or high energy electron for emission, etc.



[1] M. Lundstrom, *Fundamentals of Carrier Transport*, Cambridge, (2000) [2] Prabhu et al. Phys. Rev. B, 51, 14233 (1995).
 [2] M. Kaviani, *Heat Transfer Physics*, Cambridge (2014) [4] S.A. Egorov and J.L. Skinner, J.Chem. Phys. **103**, 22 (1995).

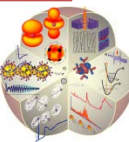


Hot phonon relaxation



(GaAs, $\Delta t = 10$ fs)

- The population of LO phonons decreases while population of phonons in other modes increases.
- In the early period (~ 1 ps), the number of electrons with lower energy than barrier decreases and high energy electrons are more populated. Later, the electron distribution is recovering to initial distribution.

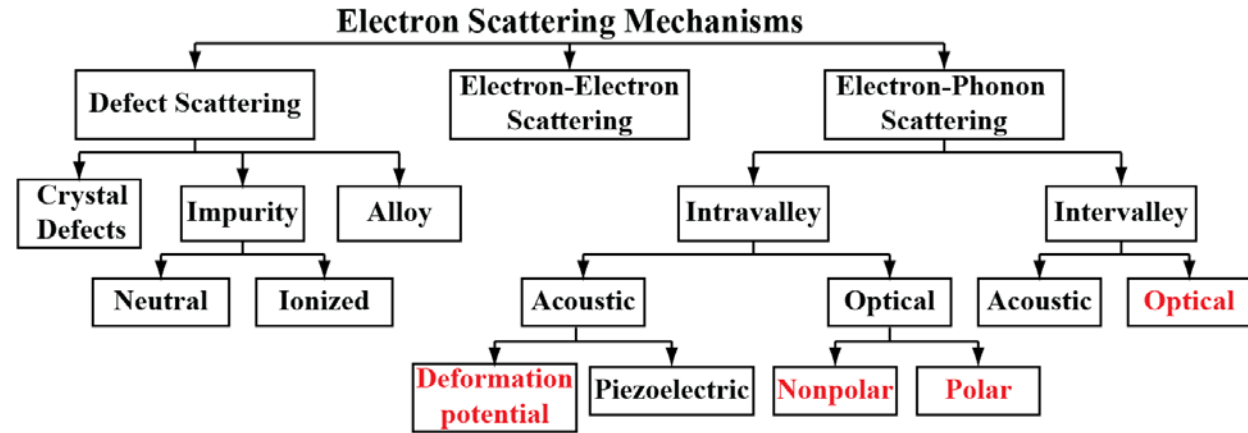


Monte Carlo (MC) Simulations

Monte Carlo method - simulate **electron transport** and **phonon absorption/emission** with **randomly selected scattering mechanisms and times**

1. Simulated carriers

- electrons in the lowest conduction band (in Γ , L, and X valleys)



2. Included interactions (in red in the chart)

- **Acoustic** phonon scattering, absorption and emission of **polar optical** phonons in each valley (Γ , L or X), and **intervalley** phonon absorption and emission ($\Gamma \rightarrow$ L or X, $L \rightarrow \Gamma$, L or X, and $X \rightarrow \Gamma$, L or X)

3. Classical equations of motion

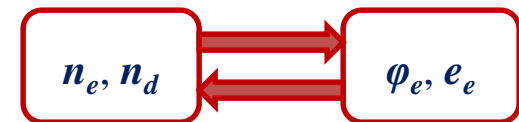
$$\frac{d\mathbf{r}}{dt} = \frac{1}{\hbar} \nabla_{\mathbf{k}} e_e(\mathbf{k}(t)) ; \quad \frac{d\mathbf{k}}{dt} = \frac{q\mathbf{e}_e(\mathbf{r})}{\hbar}$$

4. Self-consistent ensemble MC

- large **ensemble** of sampled electrons coupling to the **Poisson equation** to reflect the **internal charge redistribution**

Poisson equation (n-type)

$$-\nabla \cdot (\epsilon \nabla \phi) = 4\pi \rho_e, \quad \rho_e = -e(n_e - n_d)$$



[1] R. W. Hockney and J W Eastwood, "Computer simulation using particle", Adam Hilger (1988)

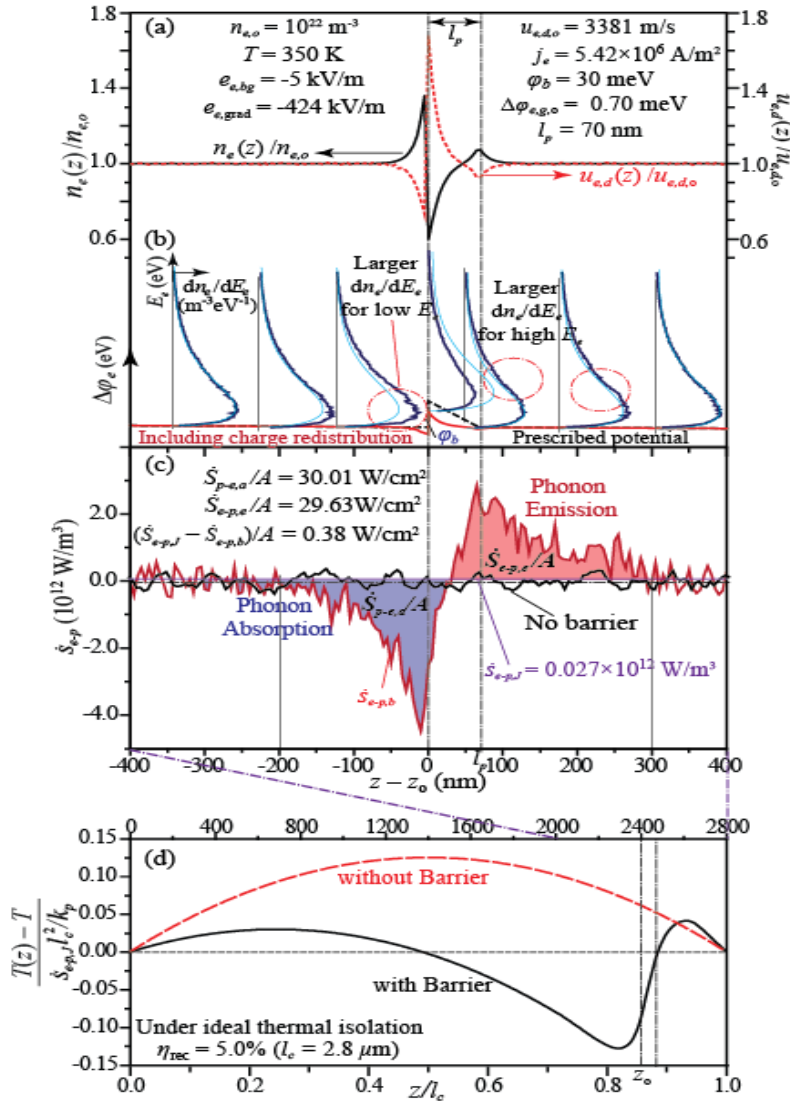
[2] C. Jacoboni and P. Lugli, "The Monte Carlo Method for Semiconductor Device Simulation", Springer-Verlag (1989)

[3] C. Moglestue, "Monte Carlo Simulation for Semiconductor Device", Chapman & Hall (1993)

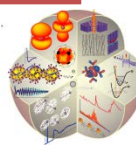
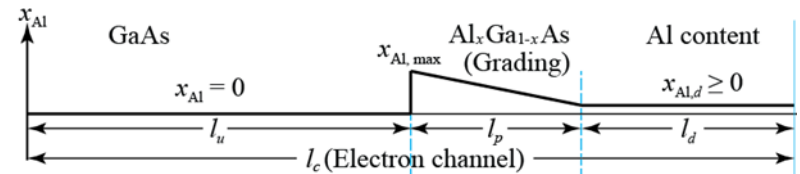
[4] K. Hess, "Monte Carlo Device Simulation: Full Band and Beyond", Kluwer Academic Publishers (1991)



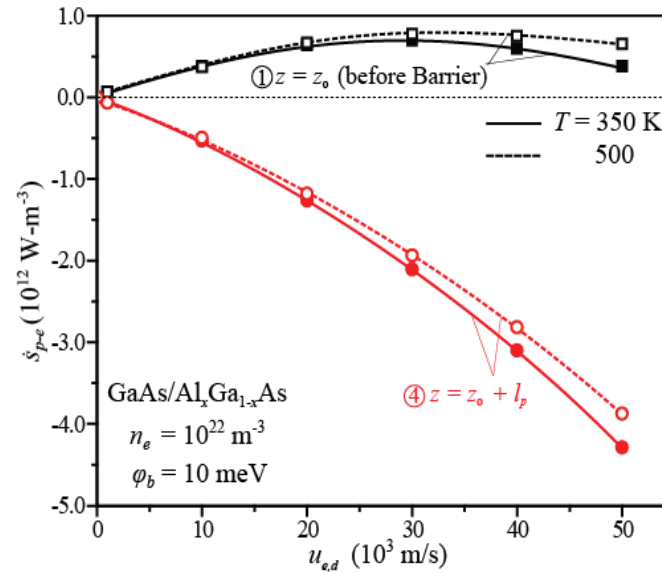
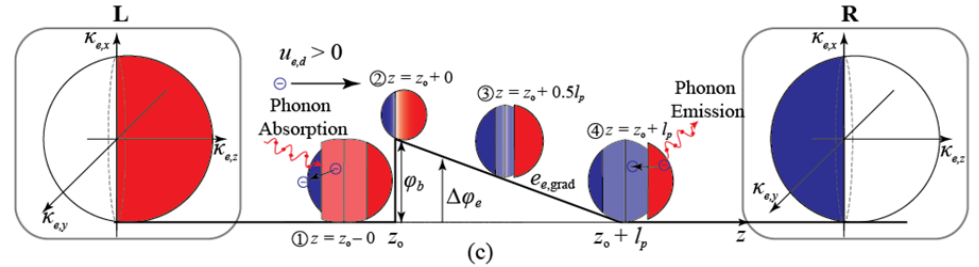
MC Simulation - Particle/Velocity/Potential/Electron Energy Distribution



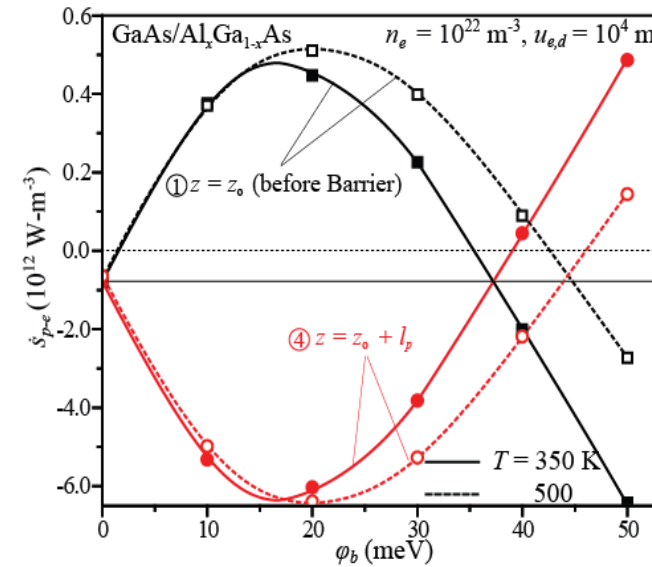
Spatial variations of (a) electron population and velocity, (b) electron energy distribution and electric potential, and (c) the net phonon emission rate. Since the low-energy electrons are overpopulated due to the barrier, large phonon absorption occurs upstream of the barrier, large phonon emission occurs upstream of the barrier. (d) The temperature distributions under ideal thermal isolation with and without the barrier. The phonon recycling efficiency is also listed. Using the phonon emission from MC, the temperature is calculated. The recycling reduces the net phonon emission and the channel temperature.



Phonon Absorption and Emission Rates



(a)

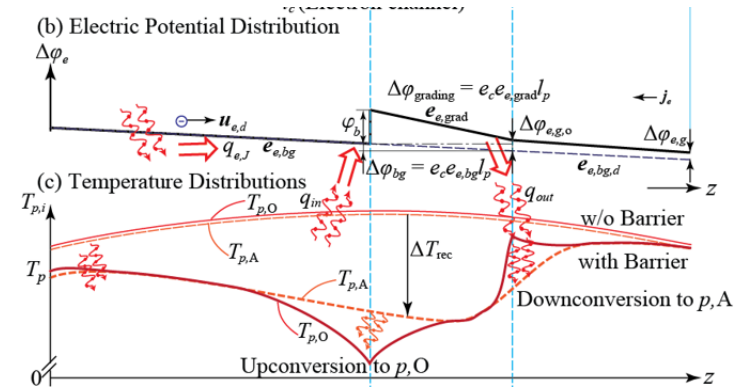
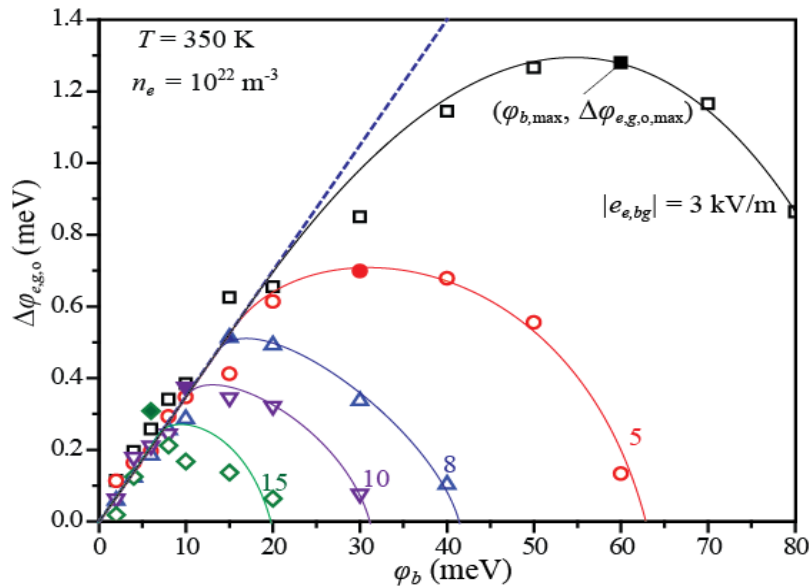


(b)

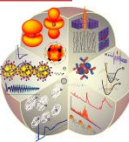
Variations of the net phonon absorption rates with respect to (a) current, and (b) barrier height, for $T_e = 350$ K and 500 K at z_0 and at $z_0 + l_p$. The net phonon absorption rate (integrated net absorption rate over energy range) upstream first increases, but decreases at high currents, resulting in a smaller gain. High barrier causes more reflection, so the phonon absorption.



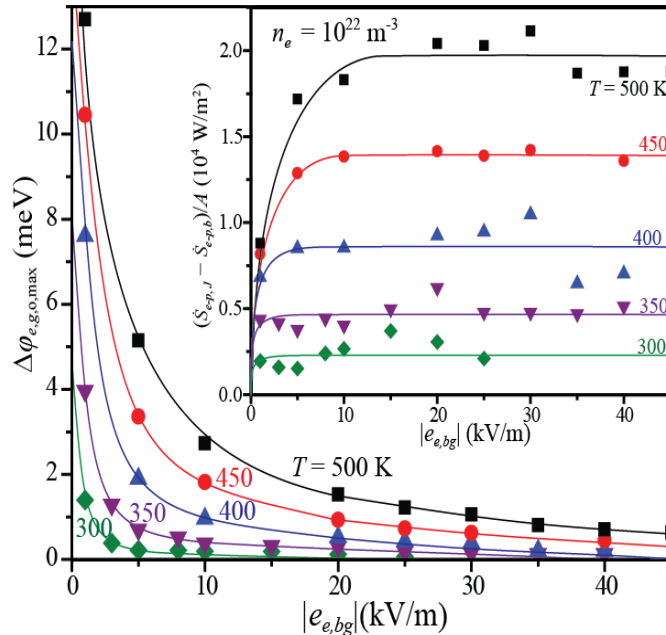
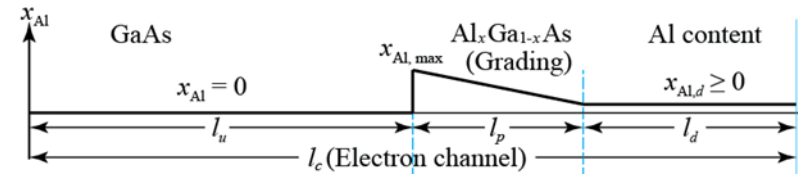
Gained Potential



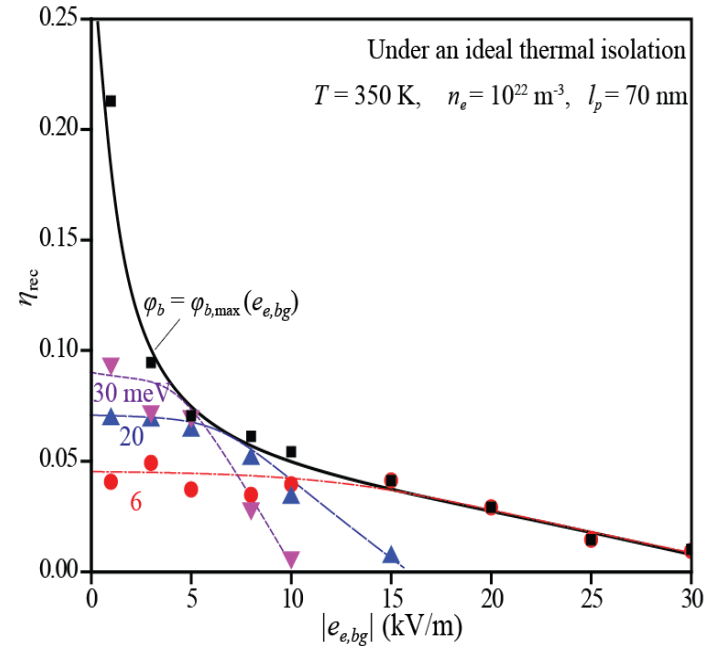
Variations of the potential gain ($\Delta\phi_{e,g,o}$) with respect to the barrier height (ϕ_b), for six background field intensities ($e_{e,bg}$). An optimal potential barrier ($\phi_{b,max}$) exists, and this $\phi_{b,max}$ decreases with $e_{e,bg}$. For a given field, the optimal barrier height, which maximizes the potential gain, exist and increases and then decreases.



Efficiency of Barrier

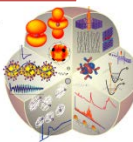


(a)

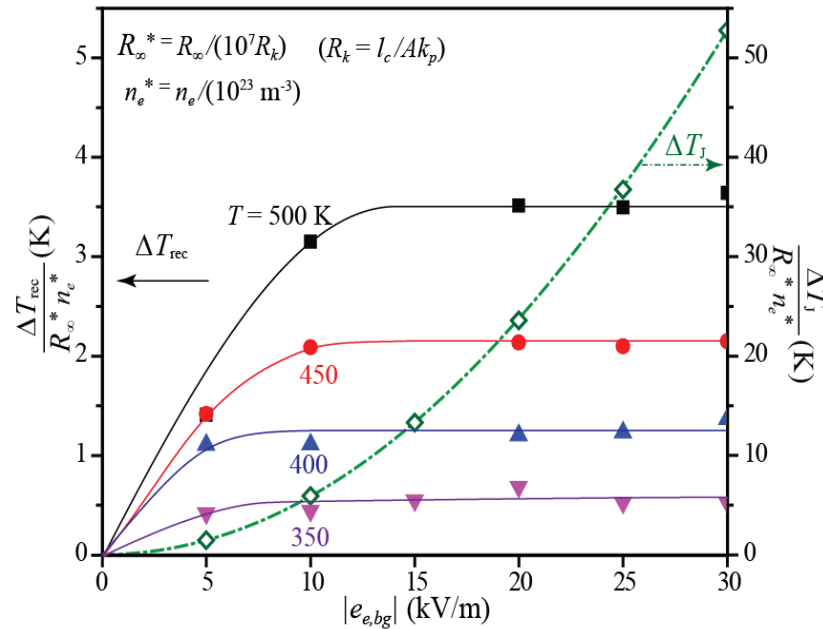


(b)

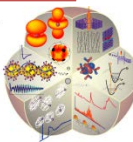
(a) Variations of the maximum potential gain ($\Delta\phi_{e,o,max}$) with respect to $e_{e,bg}$, for five temperatures. The reduction in phonon emission becomes more pronounced with increase in temperature, as shown in the inset. (b) Variations of the phonon recycling efficiency with respect to $e_{e,bg}$ for three different prescribed barrier heights (ϕ_b) and the optimal barrier height ($\phi_{b,max}$) and under ideal thermal isolation.



Self Cooling (phonon recycling using heterobarrier)



Variations of the temperature reduction by phonon recycling, as a function of background electric field ($e_{e,bg}$) and for four temperatures, under nonideal thermal isolation (finite external thermal resistance R_{∞}). The temperature rise due to joule heating without recycling is also shown to the right. This temperature reduction is improved by thermal isolation and increase in the carrier density (n_e).



3. PHONOVOLTAIC

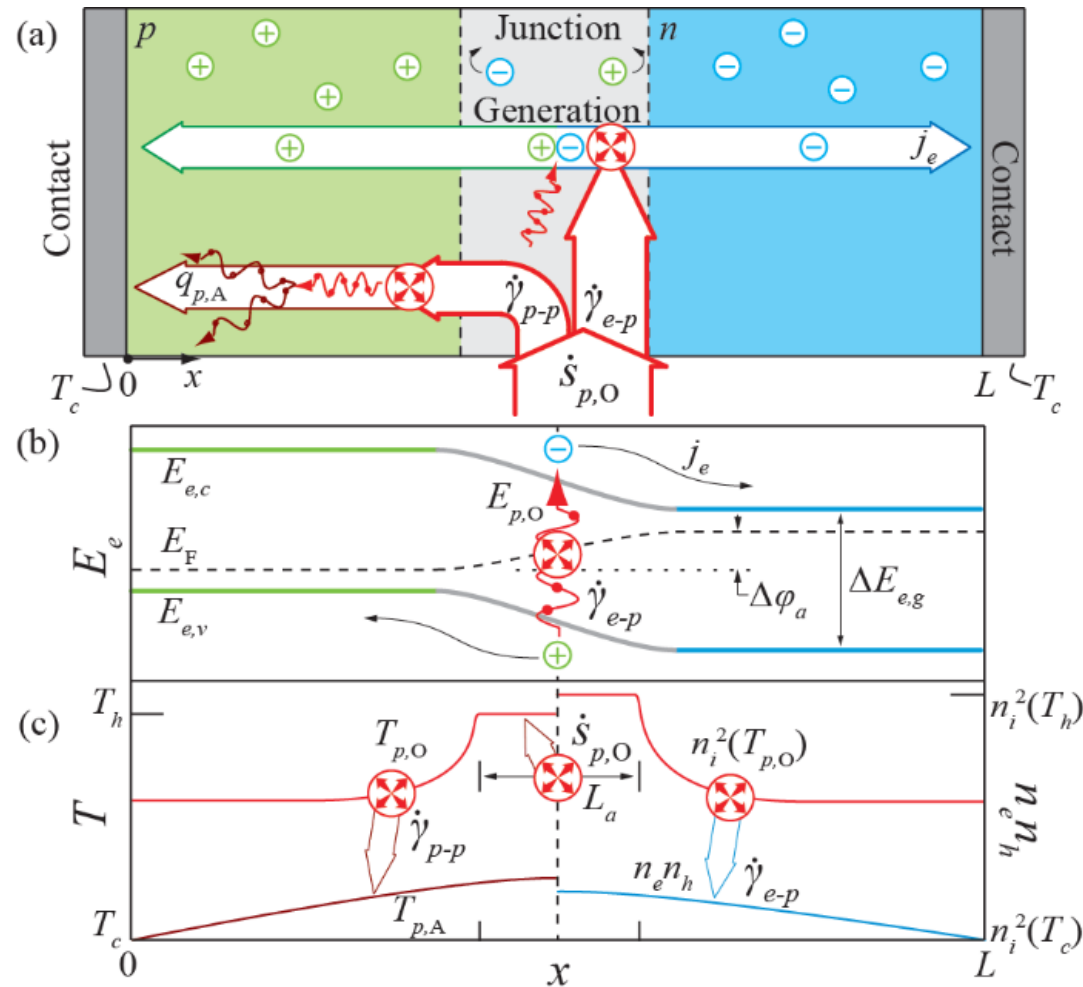
Harvest optical phonons like a photovoltaic harvests photons

Operation

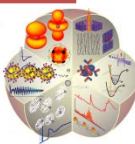
- Hot optical phonon population
- More energetic than the band gap
- Create electron-hole ($e-h$) pairs in a $p-n$ junction
- Junction field separates $e-h$ pairs
- To generate power
- Before hot phonon population down-converts into acoustic phonon modes

Challenges

- Down-conversion of optical phonons
- Lack of suitable materials
 - $E_{p,O} > \Delta E_{e,g} \gg k_B T$



(a) The phonovoltaic cell, (b) its energy diagram, (c) and local non-equilibria. The device functions like a photovoltaic, i.e., the hot optical phonon population generates electrons in a $p-n$ junction.



Nonequilibrium atomic vibration (hot phonons)

Nonequilibrium (Hot) Phonons

- Equilibrium phonon occupancy distribution
(The Bose-Einstein distribution)

$$f_p^o(E_p, T) = \left[\exp\left(\frac{E_p}{k_B T}\right) - 1 \right]^{-1}$$

- Nonequilibrium phonon distribution

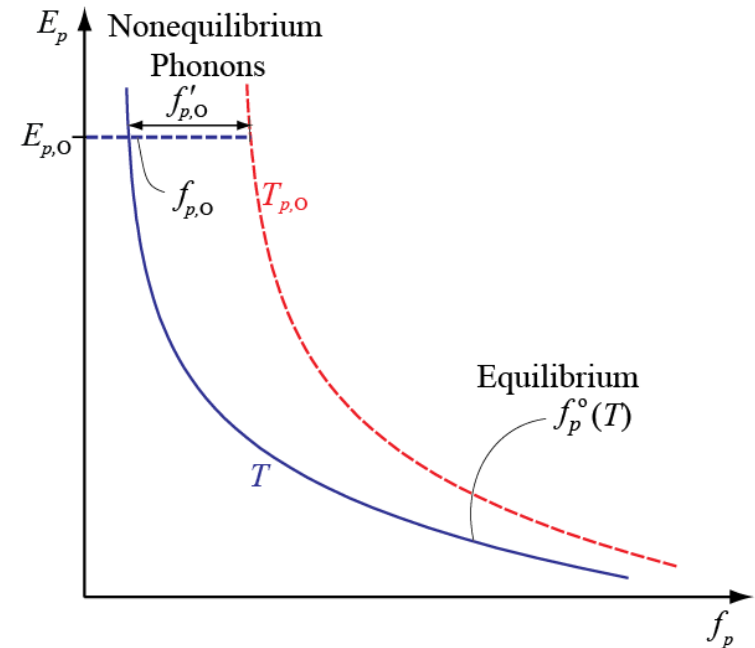
$$f_p'(E_p, T) = f_p(E_p, T) - f_p^o(E_p, T) \neq 0$$

- Nonequilibrium phonon temperature (phonon with E_p)

$$T_p(f_p, E_p) = \frac{E_p}{k_B [\ln(f_p + 1) - \ln f_p]} \quad (\text{The larger } f_p, \text{ the higher } T_p)$$

e.g., for electrons (Fermion) : $T_e(f_e, E_e) = (E_e - \mu) / \{k_B [\ln(1 - f_e) - \ln f_e]\}$

- The nonequilibrium phonons are finally relaxed by the interaction with electrons, phonons, etc.
- While interacting with electrons, the energy conversion between electrons and phonons is possible.
- Hot phonons: overpopulated phonons (normally optical phonons)



Central Mechanism

Electron-phonon coupling

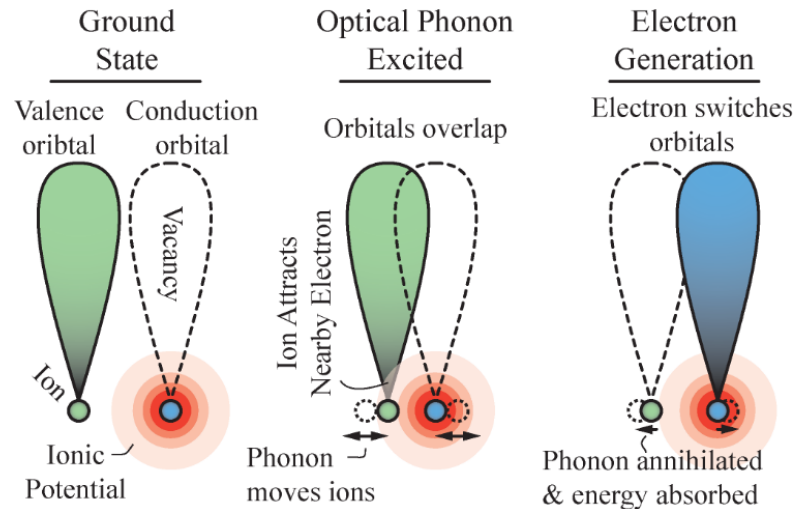
- Ion displacements effect the potential field
- Electrons can scatter with the perturbed field
- Drives electron generation

Strong coupling requires

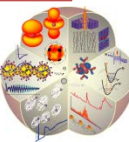
- Phonon perturbs the potential
 - Large ion motion
 - Light atoms
 - Towards/away from each other
 - Optical phonons
 - High k phonons
 - Of ions with high valence/conduction LDOS
- **Initial and final states overlap**

$$H_{e-p} = \sum_{k_e} \sum_{k_p, \alpha} \frac{1}{2} \underbrace{\left(\frac{\hbar}{2\omega_{k_p, \alpha} \langle m \rangle} \right)^{1/2}}_{\text{Linear Expansion of Perturbation}} \underbrace{\frac{\partial \phi}{\partial u_{k_p, \alpha}}}_{\text{Phonon Displacement}} \underbrace{(c_{k_e+k_p}^\dagger c_{k_e} a_{k_p, \alpha} + h.c.)}_{\substack{\text{Electron Potential} \\ \text{Absorption Emission}}}$$

Electron-Phonon Coupling



The electron phonon coupling drives generation in the phonovoltaic. A strong coupling requires that the phonon perturb the electric potential and that the initial and final states overlap substantially.



Electron generation and recombination

- From the Hamiltonian

$$H_{e-p} = \sum_{k_e} \sum_{k_p, \alpha} \frac{1}{2} \underbrace{\left(\frac{\hbar}{2\omega_{k_p, \alpha} \langle m \rangle} \right)^{1/2}}_{\text{Linear Expansion of Perturbation}} \underbrace{\frac{\partial \phi}{\partial u_{k_p, \alpha}}}_{\text{Phonon Displacement}} \underbrace{(c_{k_e+k_p}^\dagger c_{k_e} a_{k_p, \alpha} + h.c.)}_{\substack{\text{Electron Potential} \\ \text{Absorption Emission}}}$$

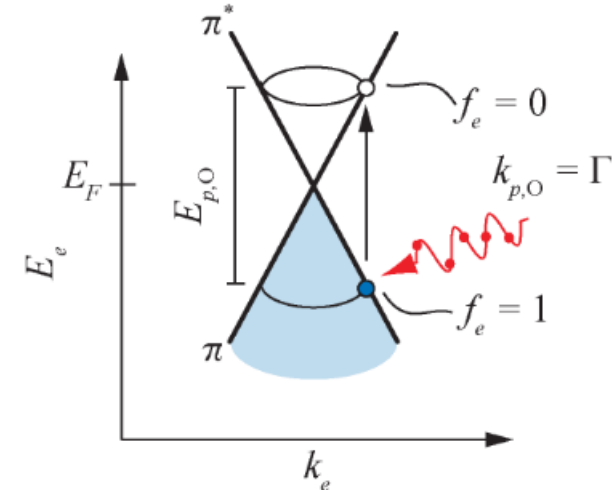
- Matrix element [1]:

$$M_{k_e+k_p, j, k_e, i} = \left(\frac{\hbar}{2\omega_{k_p, \alpha} \langle m \rangle} \right)^{1/2} \langle \mathbf{k}_e + \mathbf{k}_p, j | \frac{\partial \phi}{\partial u_{k_p, \alpha}} | \mathbf{k}_e, i \rangle$$

- Rate, from Fermi Golden Rule:

$$\begin{aligned} \dot{\gamma}_{e-p} &= \frac{2\pi}{\hbar} |M_{k_e+k_p, j, k_e, i}|^2 \\ &\times \delta(E_{e, k_e, i} - E_{e, k_e, j} \pm \hbar\omega_{k_p, \alpha}) \\ &\times (f_{p, 0} - f_{h, k_e, i} f_{e, k_e+k_p, j}) \end{aligned}$$

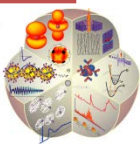
- Generation and recombination based on population term



[2] Electron – phonon interaction in graphene at 0 K for a zone-center phonon.

[1] S. Baroni, S. de Gironcoli, and A. Dal Corso, *Rev. Mod. Phys.*, **73**, 515 (2001).

[2] K. M. Borysenko *et al.*, *Phys. Rev. B.*, **81**, 121412(R) (2010).



Condition for generation, Carnot Limit, and Limiting Voltage

Generation occurs when:

$$f_{p,O} - f_h(E_h) f_e(E_{p,O} - \Delta E_{e,g} - E_h) > 0$$

Assuming $f_e = f_e^0$ and a non-degenerate semiconductor:

$$\exp\left(\frac{-E_{p,O}}{k_B T_{p,O}}\right) - \exp\left(\frac{-E_{p,O}}{k_B T_e}\right) > 0$$

Thus, the condition for generation is

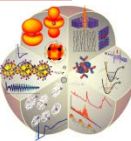
$$T_{p,O} > T_e$$

As soon as generation starts, however, the quasi-fermi level will split between electron and hole populations
Generation stops when this gets too large (**open circuit voltage**):

$$\exp\left(\frac{-E_{p,O}}{k_B T_{p,O}}\right) - \exp\left(\frac{-E_{p,O} + \Delta\phi_{oc}}{k_B T_e}\right) = 0$$

$$\Delta\phi_{oc} = \left(\frac{T_{p,O} - T_e}{T_{p,O}}\right) E_{p,O} = \eta_C E_{p,O}$$

In reality, assumption of $f_e = f_e^0$ doesn't generally hold, especially as $\Delta\phi \rightarrow \Delta E_{e,g}$



Current-Voltage Curve and Efficiency

In a more conservative model, the **open circuit voltage is limited by the band gap**, rather than the phonon energy

- The band-to-band recombination [1]

$$\dot{\gamma}_{e-p} \propto n_i^2(T_{p,O}) - n_e(T_e)n_h(T_e) \propto \exp\left(\frac{-\Delta E_{e,g}}{k_B T_{p,O}}\right) - \exp\left(\frac{-\Delta E_{e,g} + \Delta\phi}{k_B T_e}\right)$$

Gives **open-circuit voltage**

$$\Delta\phi_{oc} = \eta_C \Delta E_{e,g}$$

Phonovoltaic preserves a **fraction of the optical phonon energy**

$$\eta_\phi = \eta_C \frac{\Delta E_{e,g}}{E_{p,O}}$$

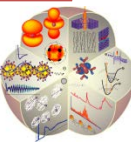
With **quantum efficiency** at short circuit

$$\eta_{QE} = \frac{\dot{\gamma}_{e-p}}{\dot{\gamma}_{e-p} + \dot{\gamma}_{p-p}} = \dot{\gamma}_{e-p}^* \quad [q_{in} = E_{p,O}(\dot{\gamma}_{e-p} + \dot{\gamma}_{p-p})]$$

And **total efficiency** (with **figure of merit Z_{pV}**)

$$\eta_{pV} = \eta_{QE} \eta_\phi F_F^* = \eta_C \frac{\Delta E_{e,g}}{E_{p,O}} \dot{\gamma}_{e-p}^* F_F^* = \eta_C Z_{pV} F_F^* \approx \eta_C Z_{pV} [1 - 0.75 \exp(-\frac{\eta_C \Delta E_{e,g}}{10k_B 10})]$$

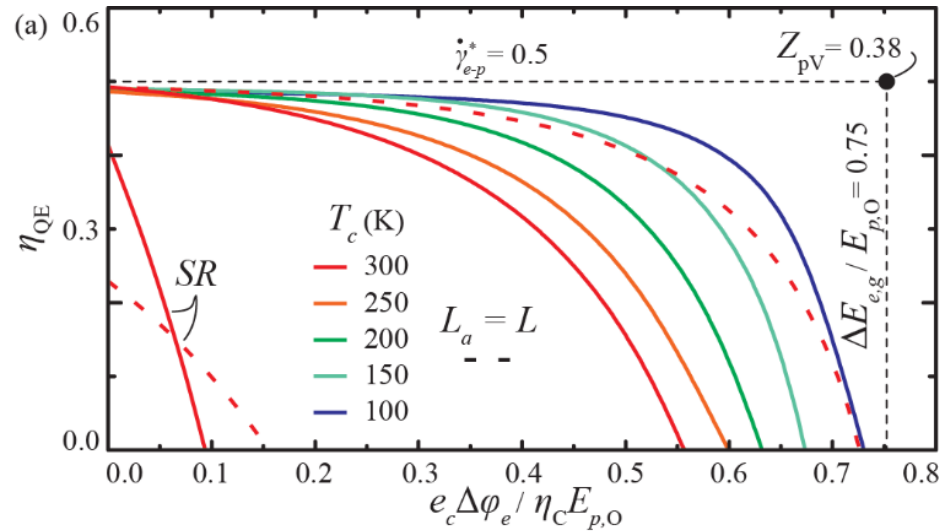
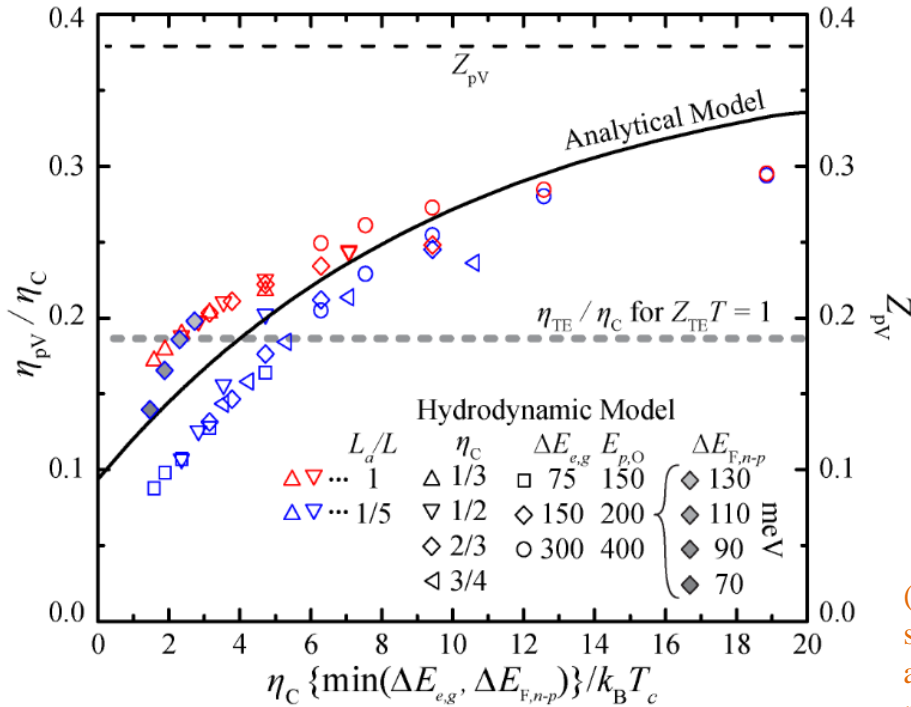
Where F_F^* is the fill factor of the current-voltage curve, adjusted by the decreasing “heat” required



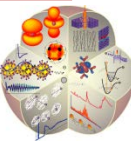
Results

This **analytical model produces accurate results**

- Analytic model vs. **hydrodynamic simulations**
- Even with analytic model using
 - Approximate fill-factor
 - Using $q(\Delta\phi=0)$
- Across wide range of parameters



(a) Dimensionless and (b) dimensional I-V curves, from hydrodynamic simulations, and (left) the resulting efficiency, as compared to the analytical model. The phonovoltaic has the exponential curve of a photovoltaic, rather than the linear curve of a thermoelectric



Primary assumption and consequences

1. The **non-equilibrium** ($T_{p,0} - T_e$) **persists** throughout the cell

- **The cell must be short!** (~ 100 nm)

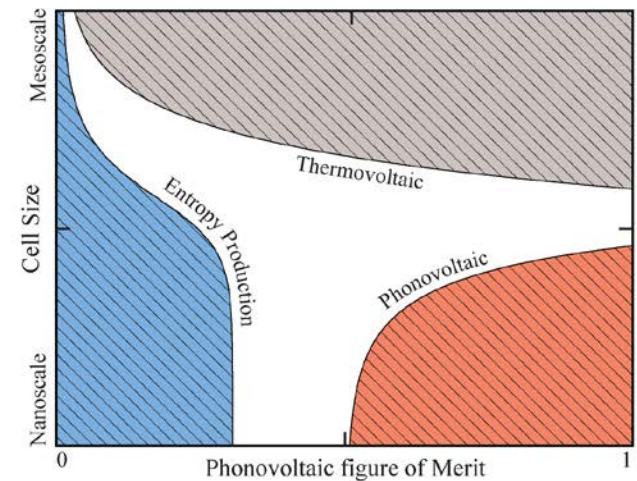
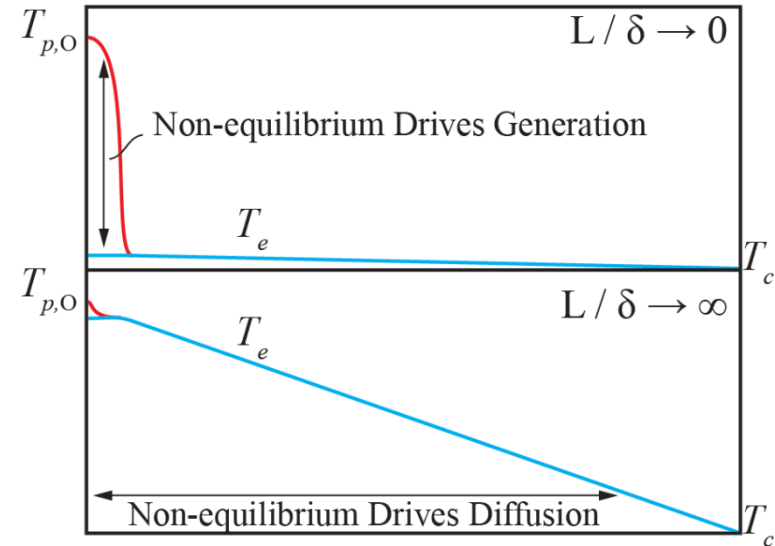
$$\Delta T_{e-p}(x) \approx \Delta T_{e-p}(0) \exp(-L / \delta)$$

$$\delta = v_e / \dot{\gamma}_{e-p}$$

- Otherwise:
 - Local Carnot is negligible
 - Generation is slow
 - Thermalization occurs
 - Spatial Carnot (∇T) is substantial
 - Heat flow
 - Electron diffusion
 - So-called **thermovoltaic**

- **Thermovoltaic** [1-4]

- Generation still occurs
 - To replace diffusive current
- Generated carriers equilibrate with $T_{p,0}$
- Heat flow
 - ∇T_e
 - $\nabla T_{p,A}$
- **Essentially a Thermoelectric device**
 - Generation instead of p-m-n junction!



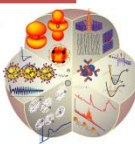
(top) Local vs. spatial non-equilibrium. A local non-equilibrium leads to phonovoltaic effects, while a spatial non-equilibrium leads to thermoelectric effects, s.t., there are (bottom) the operational regimes and the phonovoltaic must remain a nanoscale device.

[1] G. Span *et al.*, *Phys. Stat. Sol (RRL)* **1**, 241 (2007)

[2] M. Wagner *et al.*, *Semicond. Sci. and Tech.* **22**, S173 (2007)

[3] R. Chaves *et al.*, *Mat. Res. Soc. Symp. Proc.* **1543**, 3 (2013)

[4] R. Chavez *et al.* *J. Elect. Mat.* **43**, 2376 (2014)



Phonovoltaic materials

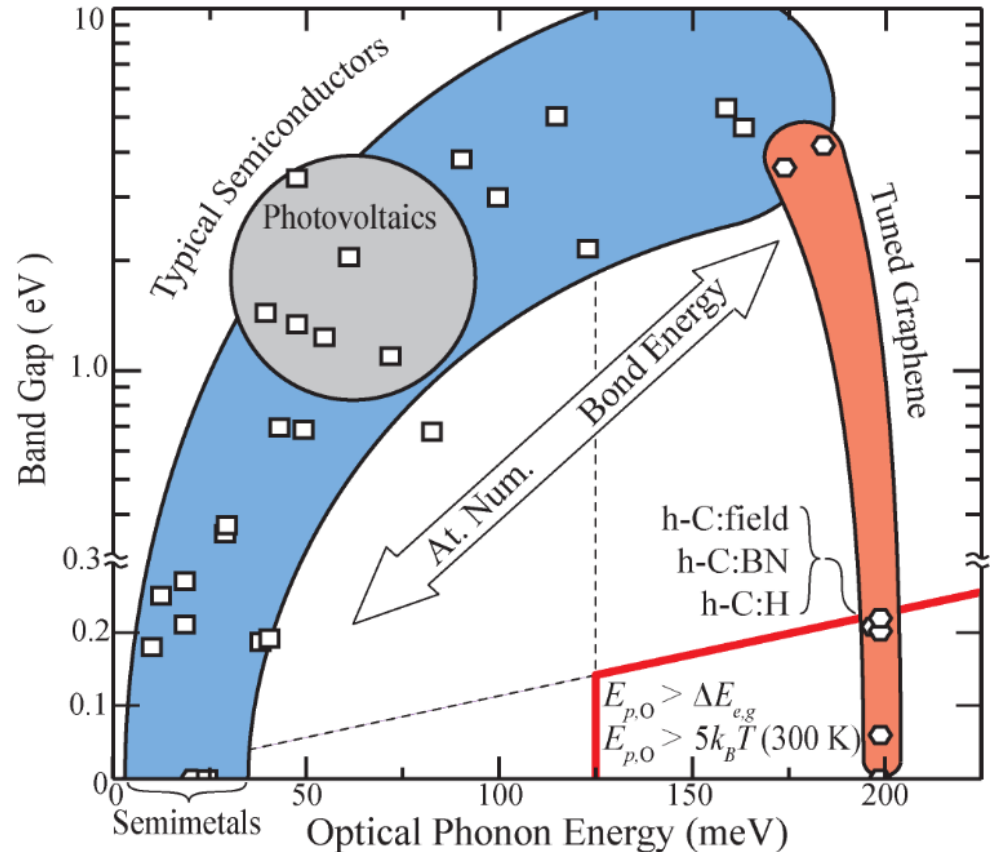
Material candidates very rare

- Primary condition ($E_{p,O} > \Delta E_{e,g}$)
 - **Typically** $E_{p,O} \ll \Delta E_{e,g}$
 - Strong bonds & light atoms
 - High $E_{p,O}$ (> 100 meV)
 - Localize electrons
 - High $\Delta E_{e,g}$ (> 2 eV)
- Secondary condition ($E_{p,O} \gg k_B T$)
 - At 300 K:
 - **Only first-row atoms**
- Third condition (e-p coupling \gg p-p coupling)
 - Further narrows field

$$Z_{pV} = \frac{\Delta E_{e,g}}{E_{p,O}} \frac{\dot{\gamma}_{e-p}}{\dot{\gamma}_{e-p} + \dot{\gamma}_{p-p}}$$

Graphene is a unique exception:

- 200 meV phonon
- Tunable band gap
- Slow thermalization
- Strong e-p coupling



Most semiconductors have extremely large band gaps compared to their optical phonon energy. Most semimetals have extremely low energy phonons. Graphene is an exception to these trends.



Tuned graphene

Graphene

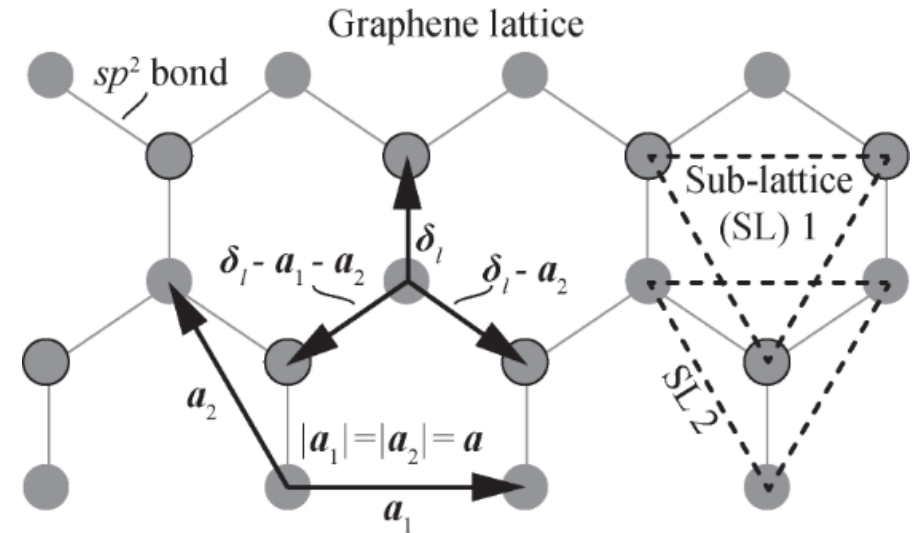
- sp^2 hybridized hexagonal lattice
- No band gap
 - Symmetric sub-lattice
 - π -bands with degenerate Dirac points

Opening a band gap in graphene

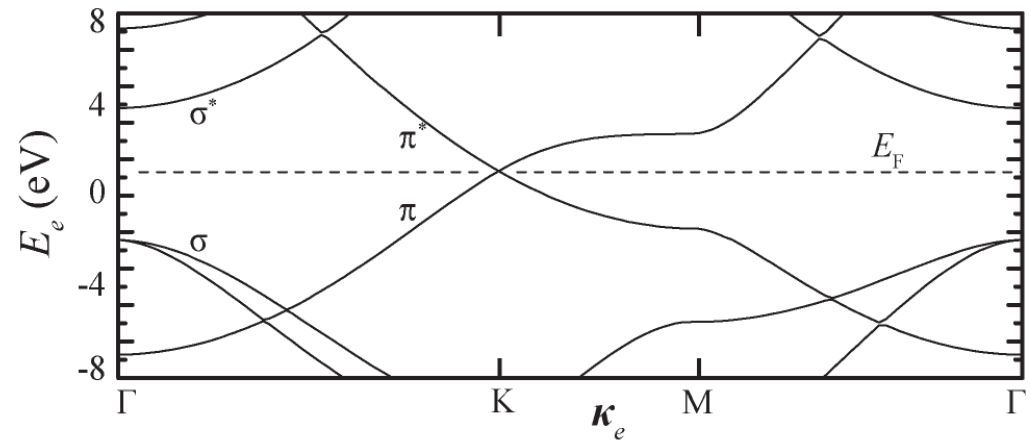
- Strain [1]
 - Extremely large strain required
- Chemical-functionalization [2], e.g.,
 - Hydrogenation (**graphane**) [3]
 - **sp^3 hybridization destroys $e-p$ coupling**
 - BN substitution (**h-C:BN**) [4]
- Electric field (**bilayer h-C + field**) [5]
- Substrate [6], e.g.,
 - BN substrate (**h-C/BN**) [6]

Changing symmetry is the most promising route

- Tune band gap with good control
- Preserve $e-p$ coupling



(Top) Graphene structure and geometry. (Left) The Brillouin zone in graphene. (Bottom) The near-Fermi band-structure. The symmetry of graphene leads to the degenerate Dirac points.



[1] F. Guinea *et al.* *Nat. Phys.* **6** 30 (2009)

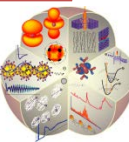
[2] V. Georgakilas *et al.* *Chem. Rev.* **112**, 6156 (2012)

[3] C. Melnick and M. Kaviani, *Phys Rev. B* **93**, 125203 (2015)

[4] R. Nascimento *et al.*, *J. Phys. Chem. C* **119** 5055 (2015)

[5] C. Park *et al.*, *Phys. Rev. Lett.* **115** 015502 (2015)

[6] P. Moon and M. Koshino, *Phys. Rev. B*, **90** 155406 (2014)



Tuned graphene – a tight-binding model

Tight-binding model

- Hamiltonian primarily sum of atomic Hamiltonians

$$H_{TB} = \sum_m H_{at,m} + \sum_{m'} \Delta H_{mm'}$$

- Wavefunction's built from combination atomic orbitals

$$\psi_{\kappa}(r) = \frac{1}{N^{1/2}} \sum_{ml} \beta_m p_z(r - R_{lm}) e^{i\kappa \cdot R_{lm}}$$

Assume

- **Orthogonal wavefunctions**
- Interacts with nearest neighbors only

$$\mathbf{H} = \begin{pmatrix} \varepsilon_{pz,1} & -\varphi_h \gamma(\kappa) \\ -\varphi_h \gamma^*(\kappa) & \varepsilon_{pz,2} \end{pmatrix}$$

$$\mathbf{H}\beta = E_n(\kappa)\mathbf{I}$$

Band gap opens when symmetry broken

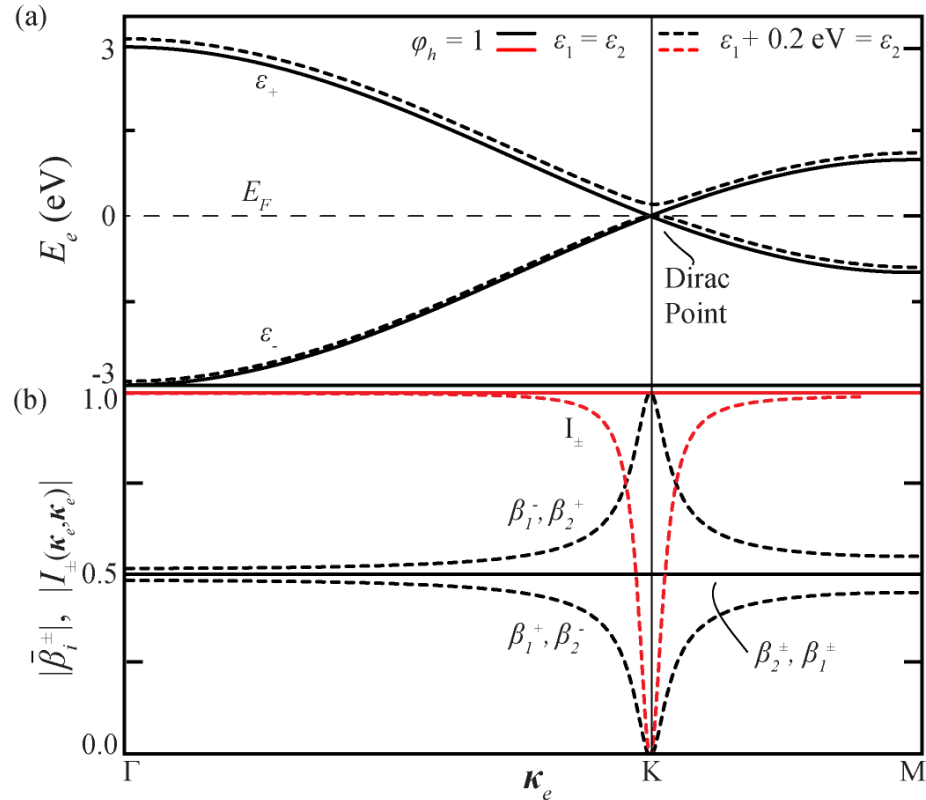
- $\varepsilon_{pz,1} \neq \varepsilon_{pz,2}$

Overlap between valence and conduction band wavefunctions vanishes at the band edge

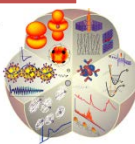
- e - p coupling proscribed at former Dirac points

- **Generation vanishes as $\Delta E_{e,g} \rightarrow E_{p,0}$**

- **Relaxes if neighboring atomic orbitals are non-orthogonal**



(a) Tight-binding band structure of graphene and tuned graphene. When the symmetry of graphene breaks, a band gap opens and the (b) wavefunctions collapse into atomic orbitals centered on one of the two-sub-lattices, s.t., the overlap vanishes.



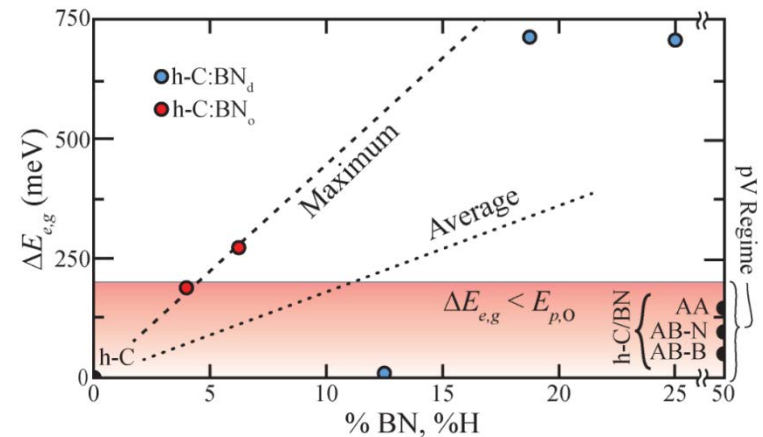
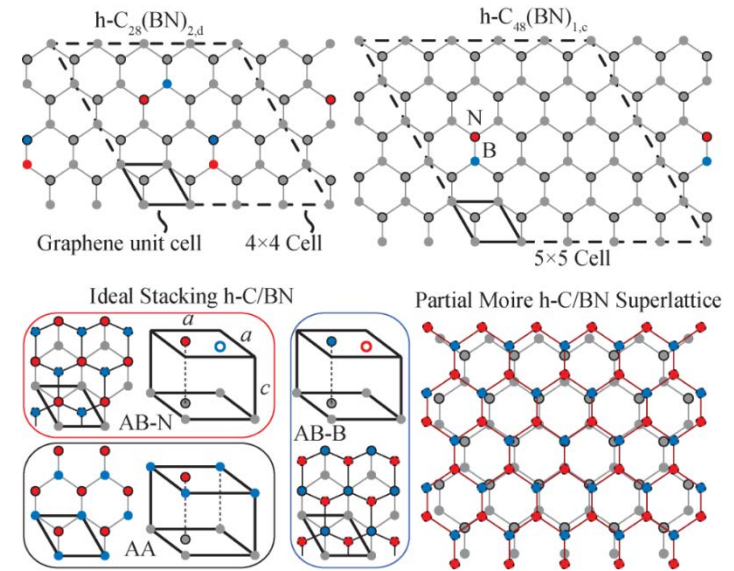
Graphene:BN & Graphene/BN

Graphene:BN [1,2,3]

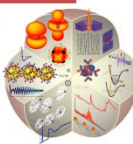
- Dilute concentration of BN substituted for C atoms in graphene
- Band gap maximized when
 - B on one sub-lattice
 - N on the other
- BN pairs/clumps very likely
- Substitution changes symmetry:
 - $\epsilon_{pz,1} \neq \epsilon_{pz,2}$

Graphene/BN [4,5]

- Graphene placed on h-BN substrate
- Band gap maximized when
 - B atoms below one sub-lattice
 - N atoms below the other
- Van der Waals interactions change symmetry:
 - $\epsilon_{pz,1} \neq \epsilon_{pz,2}$
- **Natural configuration is Moire superlattice**
 - Lattice constants are different
 - Too many atoms for *ab initio* phonon runs
- **We simulate ideal stacking configurations**
 - Phonon – phonon calculations are possible
 - More data to test TB model and investigate *e-p* coupling



(top) h-C:BN and (middle) h-C/BN crystals structures. Change in symmetry opens small band gap (bottom).



Electronic and Phononic properties

Graphene/BN

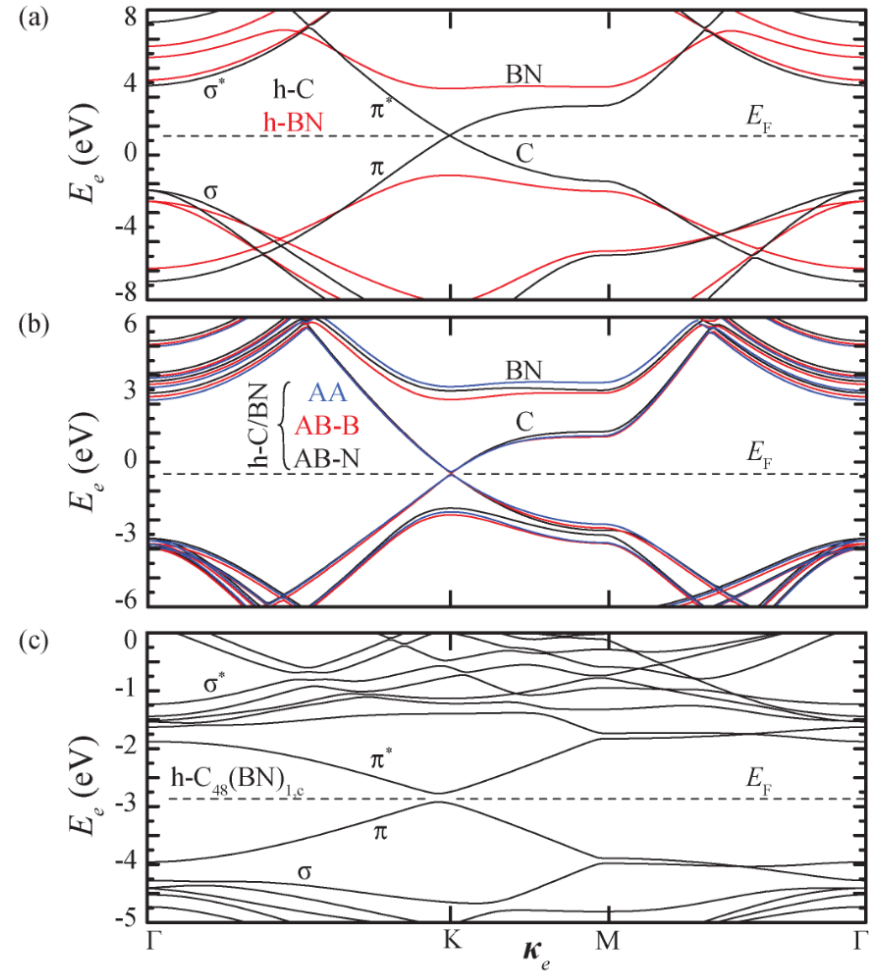
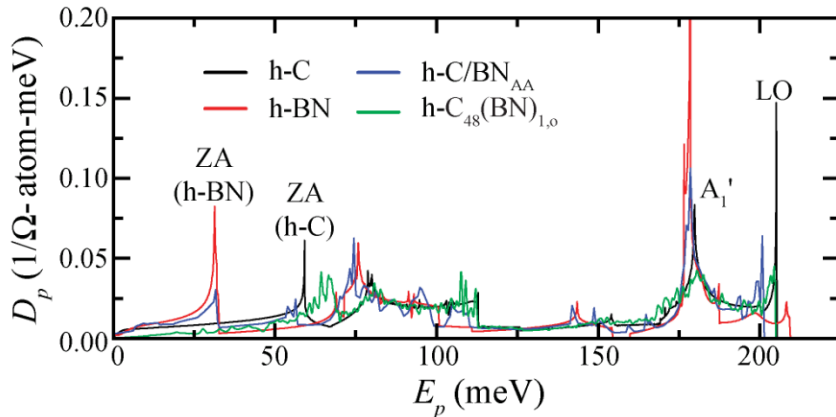
- Electron and phonon structure \approx h-C + h-BN
 - sp^2 orbitals unaffected by Van der Waals
 - Force constants unchanged
 - σ -bands unchanged

Graphene:BN

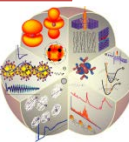
- Electron and phonon structure \approx h-C
 - Low concentration of BN
 - BN similar force constants/weight
- More substantial changes

Changes:

- π -bands near Fermi level
 - Band gap
 - Dispersion
 - **Predicted by TB model**



(Top) Band structure and phonon density of states (left) of (a) h-C and h-BN, (b) h-C/BN, and (c) h-C:BN. h-C/BN properties resemble those of h-C + h-BN with a band gap. h-C:BN properties mostly resemble those of h-C, with more substantial changes.



Electron-phonon coupling

Graphene

- Strong e - p coupling at Dirac point
- Increases along $K - \Gamma$ line
- Decreases along $K - M$ line
- Vanishes between σ bands (around Γ)

Graphene/BN

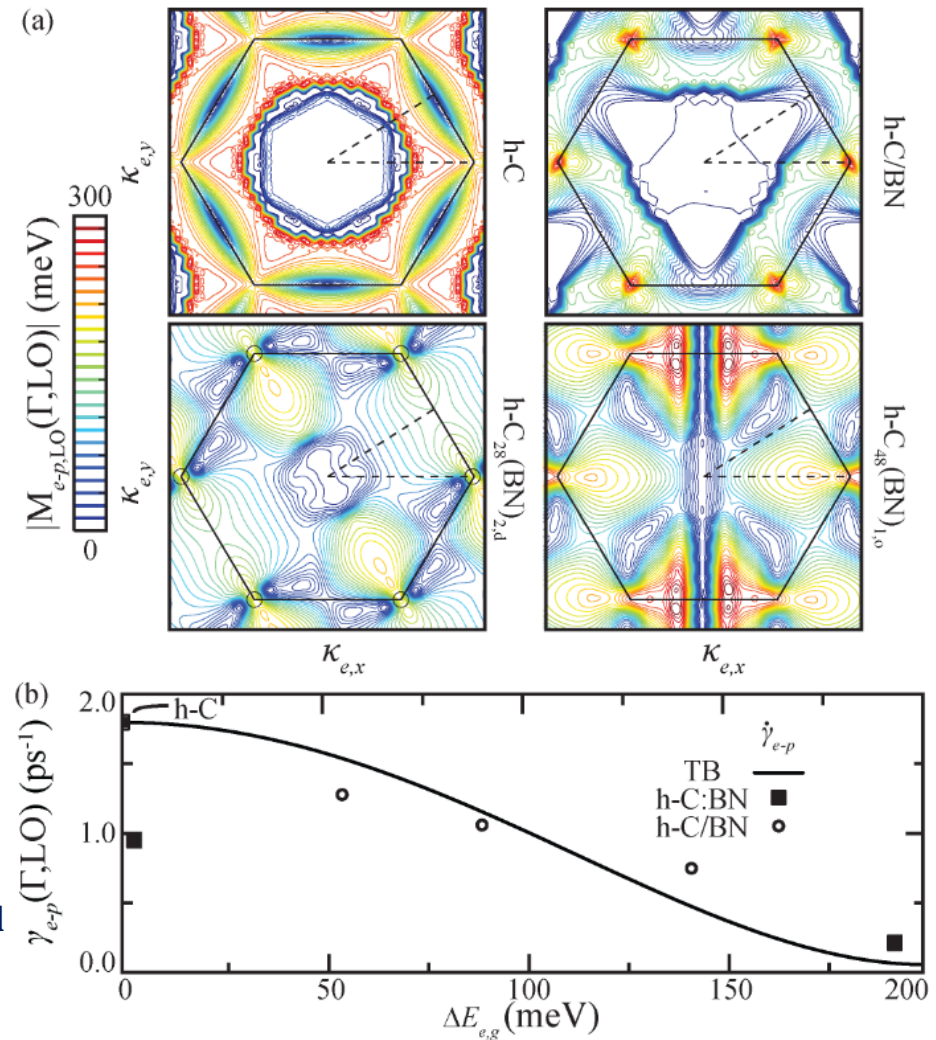
- Strongest at K point
 - Stronger than graphene
 - **Contradicts TB model**

Graphene:BN

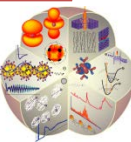
- Strong e - p coupling at former Dirac point
 - Nearly identical to graphene
 - **Contradicts TB model**
- Coupling weakens as BN concentration grows

Despite differences TB model predicts overall rate well

- Exception: high concentration of BN



(a) Electron-phonon coupling throughout the BZ in h-C, h-C/BN, and h-C:BN. Coupling remains strong at the former Dirac points, despite band gap, such that the (b) scattering rate exceeds the tight binding predictions, unless the BN concentration is high.



Bilayer-graphene under a field

Electronic structure

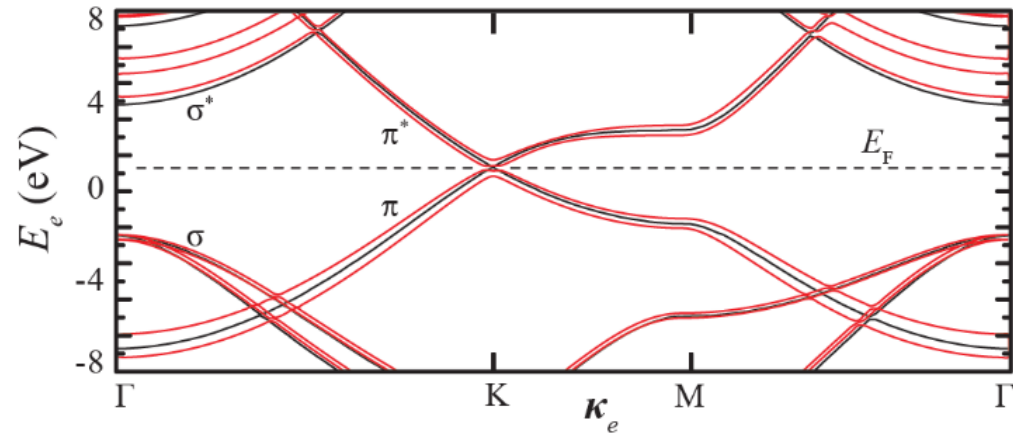
- Field pushes electrons into one of the layers
- Cross plane C-C interactions change symmetry
- Band gap opens

Unlike graphene:BN, the **e-p coupling vanishes at the K points**

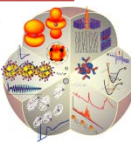
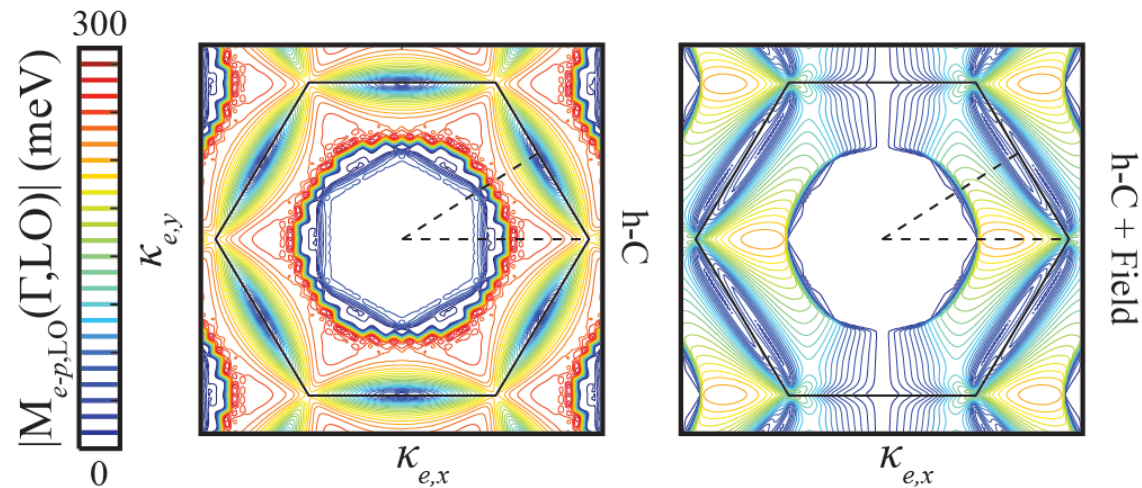
- **Agrees with TB model**

However, the **band structure changes topology around K**

- Single point \rightarrow Ring
- Number of states available for generation increases as the band gap approaches the optical phonon energy
- **Scattering rate even faster than in pure graphene**
 - **Again, TB model conservative**



(top) The band structure of graphene (black) and bilayer graphene under a field (red). The field opens a band gap and changes the topology of the band-edges. Thus, while the (bottom) e-p coupling weakens, the scattering rate is enhanced.



Phonon-phonon coupling & thermalization in graphene

Down-conversion comes from anharmonic effects

$$H_c = H_o + \sum_{ij,xy} \Gamma_{ij}^{xy} d_i^x d_j^y + \sum_{ijk,xyz} \Psi_{ijk}^{xyz} d_i^x d_j^y d_k^z + \dots$$

Ground state
Force constants
Anharmonic terms

Ab initio p-p calculation computationally expensive

• **Limited to 4 atoms or fewer**

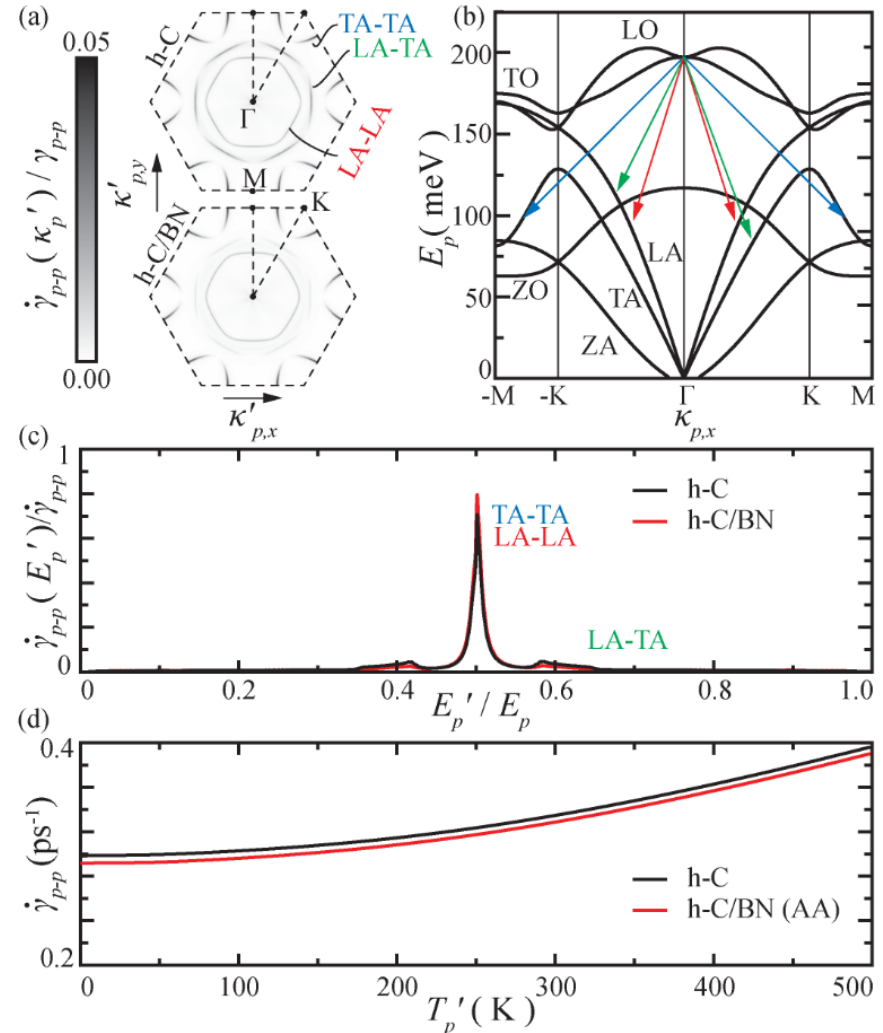
- Graphene
- Graphene/BN

Graphene

- Three pathways for down-conversion
- Energetic final modes ($E_{p,O}/2$)
 - Slow thermalization (~ 3 ps lifetime)
 - Up to high temperatures

Graphene/BN

- **Nearly identical to graphene**
 - Slightly suppressed LA-TA pathway
 - Same reasons phonon DOS is similar
 - sp^2 bonds unaffected by change in symmetry



(a) Phonon-phonon coupling throughout the BZ, (b,c) down-conversion pathways, and (d) resulting down-conversion rates. Down-conversion in h-C/BN is nearly identical to that in h-C.



Phonovoltaic performance of tuned graphene

Graphene [1,2]

- If band gap is tuned to optical phonon and no other properties change:
 - goal of $Z_{pV} \approx 0.8$

Graphane [2]

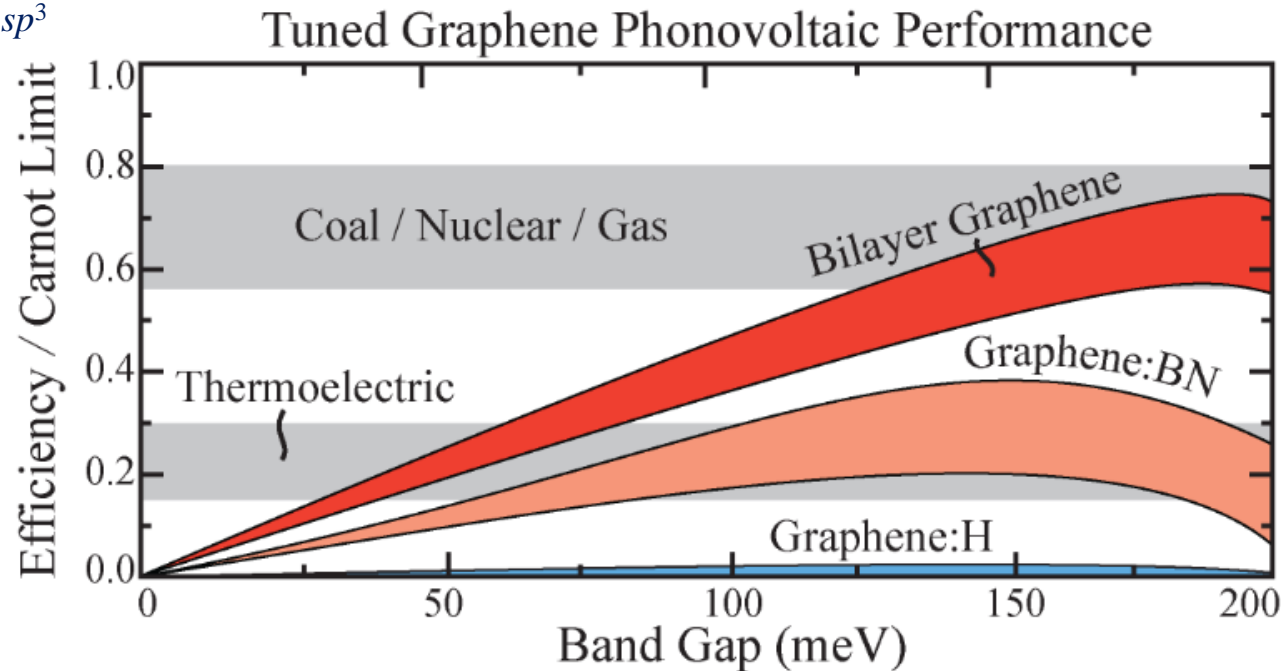
- e-p coupling vanishes as $sp^2 \rightarrow sp^3$
 - $Z_{pV} \approx 0.0$, $\eta_{pV} \approx 0.10$

Graphene:BN [3]

- e-p coupling remains strong
- Number of states decreases
 - $Z_{pV} \approx 0.5$, $\eta_{pV} \approx 0.13$
- Exceeds thermoelectric efficiency

Graphene + Field [4]

- e-p coupling remains strong
- Number of states increases
 - $Z_{pV} \approx 0.95$
 - $\eta_{pV} \approx 0.35$
- Nears conventional heat harvest efficiencies at the nanoscale



Efficiency in phonovoltaic cells can exceed 60% of Carnot, if the figure of merit is sufficiently high, even at 300 K.

[1] C. Melnick and M. Kaviani, *Phys Rev. B* **93**, 094302 (2015)
[2] C. Melnick and M. Kaviani, *Phys Rev. B* **93**, 125203 (2015)
[3] C. Melnick and M. Kaviani, *Phys Rev. B* (submitted 2016)

[4] Current work



Bilayer-graphene field-effect transistor with in-situ phonovoltaic cell (FET-pV)

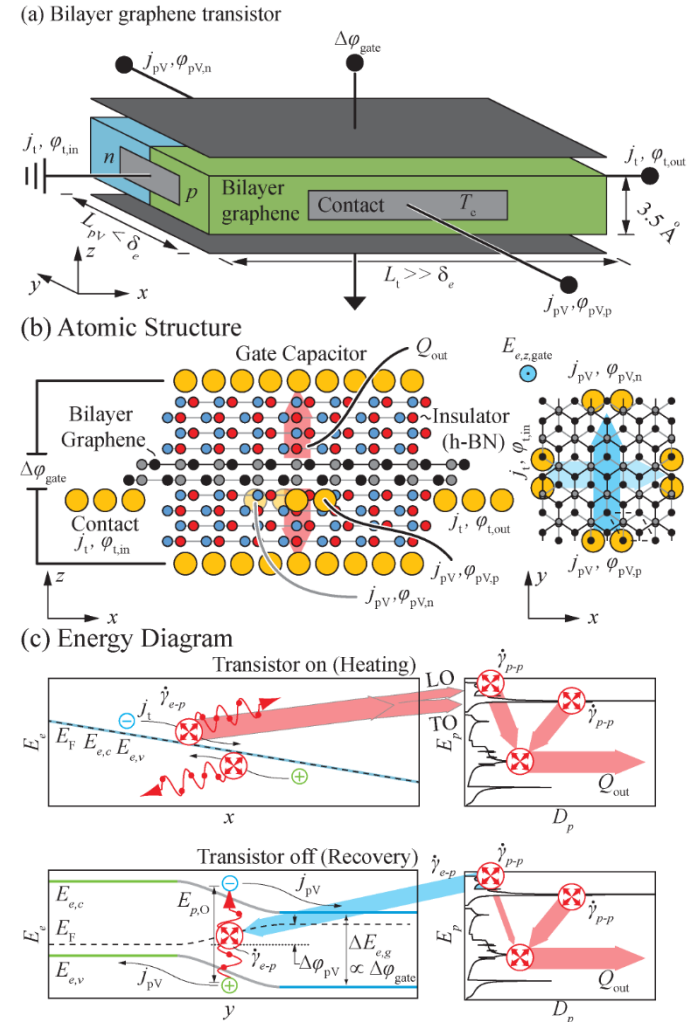
Bilayer graphene has particularly exciting Z_{pV}
 Can we design or find an application where it could shine?

Consider a bilayer-graphene FET-pV

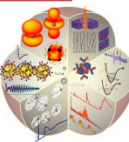
- Transistor along x
 - $p-i-n$ junction along y
 - Gate voltage applied along z
1. **Small gate voltage:**
 - Transistor voltage still drives current
 - Electrons release optical phonons
 - Hot optical phonon population created
 - Optical phonons generate electron-hole pairs before they become heat
 - $p-i-n$ junction separates electron-hole pairs to generate power
 2. **Large gate voltage**
 - stops transistor & pV current

Hypothesis:

- **Substantial reductions in heat produced**
- **Efficient power generation**



(a,b) A bilayer-graphene-transistor (c) can recycle optical phonons for power generation and reduced heat generation.



Phonovoltaic Summary

Through multiscale analysis:

1. The phonovoltaic is introduced [1].

- A “heat” harvester that mimics the photovoltaic
- An analytical efficiency and figure of merit are derived
- The potential of the cell to approach the Carnot limit is demonstrated
- The requirements for it to do so are outlined
 - Nanoscale cell
 - High figure of merit
 - Large Carnot limit
 - Large band gap compared to $k_B T$

2. Tuned graphene is shown to be the only promising material candidate [2]

- **Graphene:BN** is found as a suitable option [3]
 - ~25% of Carnot limit
 - 3D applications possible
- **Bilayer graphene** under a field is shown to be an exceptional option [Current work]
 - ~60% of Carnot limit
 - 2D applications only

3. An in-situ application is proposed:

- Bilayer-graphene FET-pV [Current work]

Indeed, the outlook is quite promising

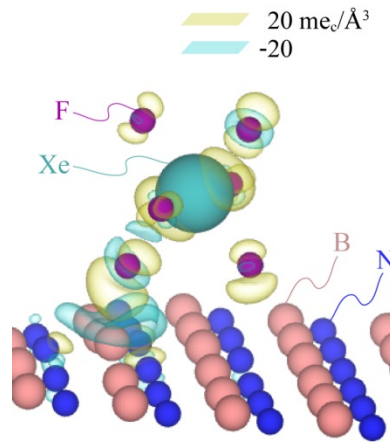
[1] C. Melnick and M. Kaviani, *Phys Rev. B* **93**, 094302 (2015)

[2] C. Melnick and M. Kaviani, *Phys Rev. B* **93**, 125203 (2015)

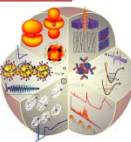
[3] C. Melnick and M. Kaviani, *Phys Rev. B* (submitted 2016)



4. PHONOCATALYSIS



We postulate and show that heterocatalysis on large-bandgap semiconductors can be controlled by surface phonons, i.e., *phonocatalysis*. With *ab initio* calculations, including molecular dynamic simulations, the chemisorbed dissociation of XeF_6 on h-BN surface leads to formation of XeF_4 and two surface F/h-BN bonds. The reaction pathway and energies are evaluated, and the sorption and reaction emitted/absorbed phonons are identified through spectral analysis of the surface atomic motion. Due to large bandgap, the vibration energy transfer channels dominate and among them is the match between the F/h-BN covalent bond stretching and the optical phonons. We show that the chemisorbed dissociation (the pathway activation ascent) requires absorption of large-energy optical phonons. Then using progressively heavier isotopes of B and N atoms, we show that limiting these high-energy optical phonons inhibits the chemisorbed dissociation, i.e., controllable phonocatalysis.



XeF₆

- XeF₆ structure
 - Xenon and Fluorine have 8 and 6 valence electrons, respectively, so XeF₆ consist of six Xe-F bonds and one lone electron pair (Molecular orbital diagram for an octahedron molecule in Fig. 1 [1]).
 - Due to the repulsive lone pair, Xe-F bonds are displaced and gaseous XeF₆ has a distorted octahedron described as Fig. 2(a) [1], and bond length and angle are changing continuously. However, XeF₄ which has a in-plane cross structure won't be distorted significantly as shown in Fig. 2(b).
- XeF₆ stability
 - XeF₆ is stable even near 1,000 K in Fig. 3 [2].

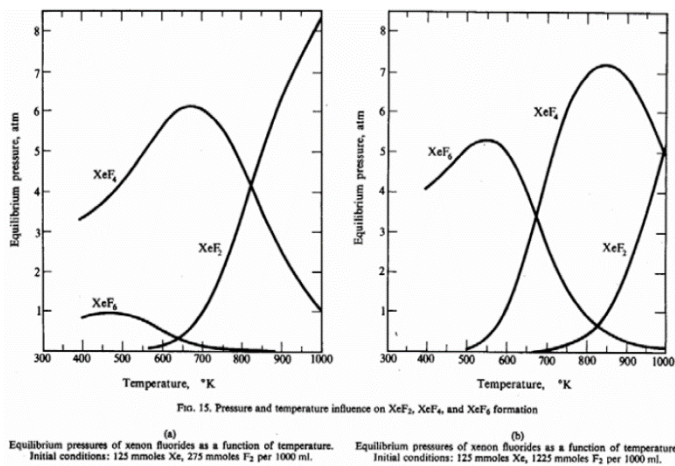


Fig. 3. Pressure and temperature effect on XeF_x population.

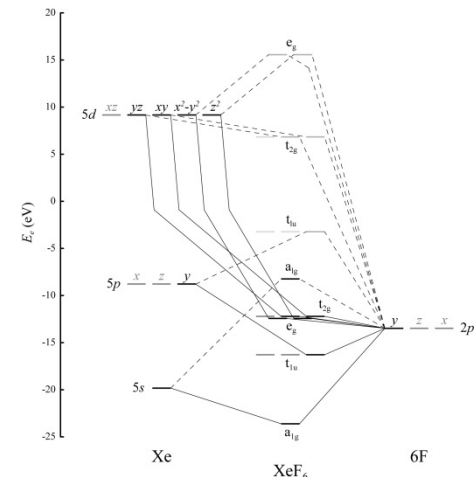


Fig. 1. Molecular orbitals (MO) for an octahedron molecule of XeF₆ with atomic orbitals of Xe and F on left and right side, respectively. Contributions of six 2p_y orbitals (occupied by only one electron) from F atoms to MO, with counterparts of Xe orbitals, are shown by linking to the bonding (solid lines) and anti-bonding (dotted lines) orbitals. MO are filled up to 2nd a_{1g} orbital. MO level is shown with y axis.

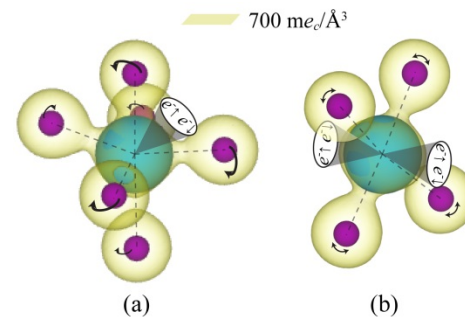
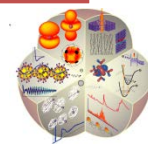


Fig. 2. Transient molecular structures of (a) XeF₆ and (b) XeF₄. The lone electron pair of XeF₆ doesn't stay at one position and thus six Xe-F bonds will show transient motion continuously around Xe atom. However, four Xe-F bonds of XeF₄ won't show intense transient motion because two lone electron pairs and four Xe-F bonds can construct intact octahedron structure.

[1] L. S. Bartell and R. M. Gavin Jr., J. Chem. Phys. 48, 2466-2483 (1968).

[2] J. C. Bailar Jr., Comprehensive Inorganic Chemistry, Vol. 1 (Pergamon Press, New York, 1973)



H-BN

- Bulk h-BN structure and properties

- Hexagonal lattice structure, like graphene. Weak van der Waals force between layers (softness) and strong covalent bond in-plane (stiffness). High in-plane mechanical strength and thermal conductivity, as well as high chemical stability even up to 1,000 °C in air.
- The calculation results show good agreement with those of previous studies for the lattice structure [1,2] and band structure and total density of states (DOS) for phonon [1-4] and electron [5-7] for bulk h-BN structure. The result shows h-BN is a large-bandgap indirect semiconductor (4.01 eV). Although there is no clear consensus for the bandgap energy (3.6~7.1 eV) as well as the type of semiconductor (direct or indirect) [5,8] and the experimental evidence of direct bandgap also suggested [8], most of theoretical predictions suggest that h-BN is a indirect bandgap material [5-7,9]. The direct interband transition is expected to be occur at M-point with the lowest direct-bandgap energy of 4.45 eV, corresponding to the ultraviolet wave and much higher than the phonon energy.

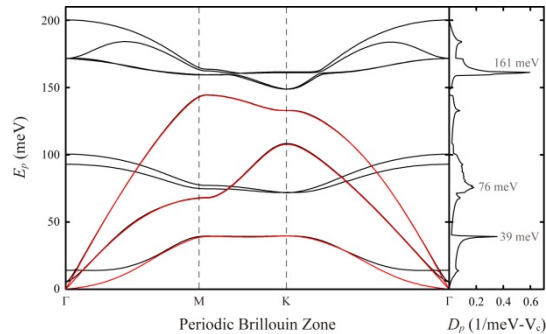


Fig. 5. Phonon band structure and total DOS of bulk h-BN structure. The red lines is for acoustic phonon modes. Phonon cut-off energy and high-energy optical phonon peak are at 200 meV and 161 meV, respectively, and low-energy acoustic phonon peak is at 39 meV. There is a very narrow bandgap near 150 meV.

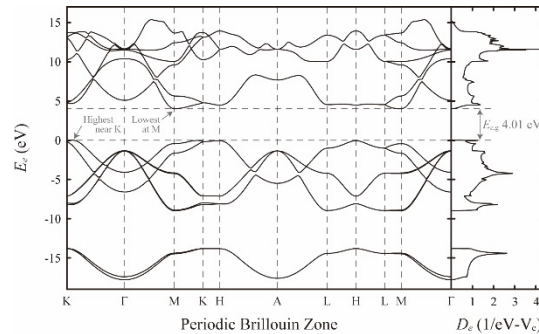


Fig. 6. Electron band structure and total DOS of bulk h-BN structure. Fermi energy is set to zero. The valence-bands maximum is near K-point and the conduction-bands minimum is at M-point, resulting in bandgap energy ($E_{e,g}$) of 4.01 eV. The lowest direct bandgap is at M-point (4.45 eV).

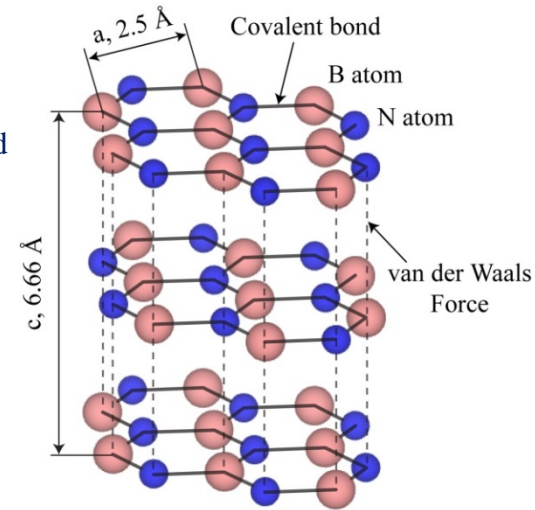


Fig. 4. Bulk h-BN structure. Cross-plane lattice constant is much larger than that in-plane due to the weak Van der Waals force. Hence, in-plane lattice vibration is much intense than cross-plane vibration.

h-BN	<i>Ab Initio</i>	Experiment
Lattice Constant		
In-plane, a (Å)	2.49 2.49 [1] 2.50 [2]	2.50 [1]
Cross-plane, c (Å)	6.45 6.48 [1] 6.51 [2]	6.66 [1]

Table 1. AI prediction of lattice constants of h-BN. The result is quite similar to ref. [1,2] and experimental data [1].

[1] G. Kern, G. Kresse, and J. Hafner, Phys. Rev. B 59, 8551 (1999).

[2] L. Wirtz, A. Rubio, R.A. Concha, and A. Loiseau, Phys. Rev. B 68, 045425 (2003).

[3] J. Serrano, A. Bosak, R. Arenal, M. Krisch, K. Watanabe, T. Taniguchi, H. Kanda, A. Rubio, and L. Wirtz, Phys. Rev. Lett. 98, 095503 (2007).

[4] H. Sevincli, W. Li, N. Mingo, G. Cuniberti, and S. Roche, Phys. Rev. B 84, 205444 (2011).

[5] L. Liu, Y.P. Feng, and Z.X. Shen, Phys. Rev. B 68, 104102 (2003).

[6] B. Altintas, C. Parlak, C. Bozkurt, and R. Eryigit, Eur. Phys. J. B 79, 301-312 (2011).

[7] R. Arenal and A. Lopez-Bezanilla, WIREs Comput. Mol. Sci. 5, 299-309 (2015).

[8] K. Watanabe, T. Taniguchi, and H. Kanda, Nat. Mater. 3, 404-409 (2004).

[9] K. Takahashi, A. Yoshikawa, and A. Sandhu, Wide Bandgap Semiconductors (Springer-Verlag, Berlin, 2007).



Reaction pathway

- Reaction pathway
 - Climbing Image Nudged Elastic Band (CI-NEB) method was adopted for reaction pathway [1-3].
 - The energy required to dissociate F atom is 0.372 eV, the activation energy between the transition state (TS) and II state.
 - Energy is released as F/h-BN bonds and XeF_4 are developed, and overall reaction is exothermic.

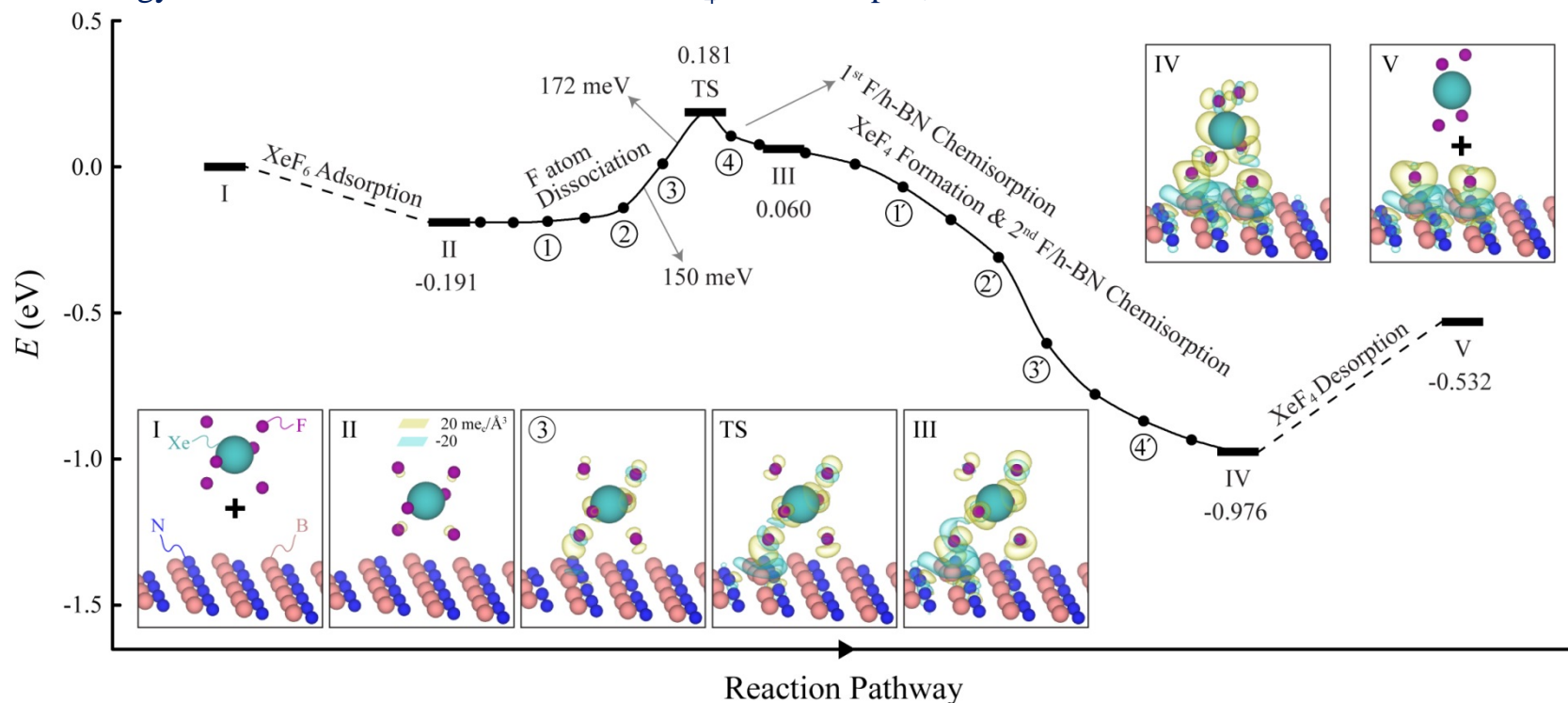
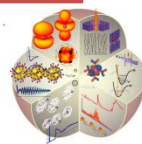


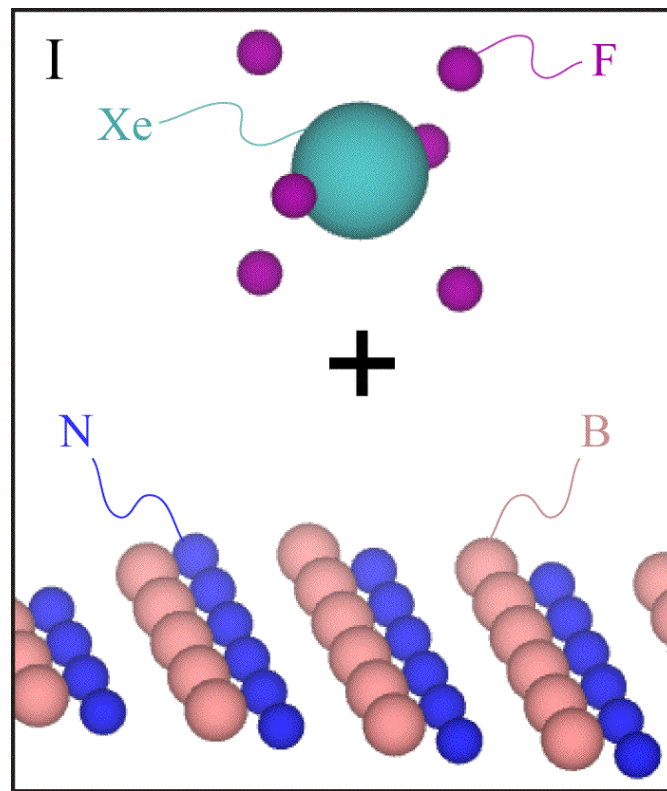
Fig. 11. Reaction pathway for XeF_6 adsorption, F/h-BN chemisorption, and XeF_4 desorption, with snapshots with distributions of charge density difference. CI-NEB was implemented between the states II & III and III & IV with 9 and 4 images, respectively. TS due to the F atom dissociation can be seen only in the 1st chemisorption. Note that circular numbers corresponds to the number of snapshots as well as that in the snapshot movie.

- [1] G. Henkelman, B. P. Uberuaga, and H. Jonsson, *J. Chem. Phys.* 113, 9901-9904 (2000).
- [2] Y-G Wang, D Mei, V-A Glezakou, J. Li, and R. Rousseau, *Nat. Commun.* 6, 6511 (2015).
- [3] M. Garcia-Melchor and N. Lopez, *J. Phys. Chem. C* 118, 10921-10926 (2014).



Mechanisms

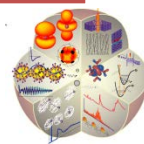
- Reaction pathway (continued)
 - The activation energy for dissociating F atom is 372 meV, and there is a steep activation ascent from near ② and TS which corresponds to the energy about 320 meV or so. It is expected that the gradual climbing from II to near ② can be easily achieved by absorbing plentiful 39 meV phonon energy, the acoustic phonon peak which can be seen in the h-BN DOS. To complete the dissociation process, it is required to overcome the steep ascent toward TS by absorbing remainder energy of 333 meV. It is also expected that this amount of energy can be provided by two-phonon contribution (e.g., two phonons of 165.5 meV) from high-energy optical phonons of h-BN because large-energy phonons around 150~180 meV can be found in h-BN (phonon peak at 161 meV and energy cut-off at 200 meV). It means, in other words, that the dissociation hardly occurs if the surface cannot provide these high-energy phonons because three-phonon interaction, whose rate is significantly lower than that of two-phonon interaction, would be needed if there is no high-energy phonon over 165.5 meV.
 - XeF_4 is formed after 1st F/h-BN bond is developed. During the XeF_4 formation, one redundant F atom is discarded and this F atom forms 2nd F/h-BN bond. This is because Xe cannot make a stable structure with 5 F atoms as shown in Fig. 2. The extra energy for dissociation of 2nd F atom is not required because the F atom disengages from the molecule spontaneously. Therefore, there is no 2nd saddle point and energy is decreasing continuously as XeF_4 and 2nd F/h-BN bond is developed during the III-IV process.
 - Comparing to the XeF_4 desorption energy on the clean h-BN surface, that on the combined system including F/h-BN bonds is much higher. This is because XeF_4 is also interacting with two F/h-BN bonds, as it can be seen in the snapshot IV that charge density difference is much larger than that in the II state (adsorption of XeF_6).



Movie 1. Movie for snapshots from reaction pathway calculation. Distributions of charge density difference show interaction of F/h-BN bonds as well as that between molecule and surface atoms. Note that numbering is coincident to that in the pathway graph.

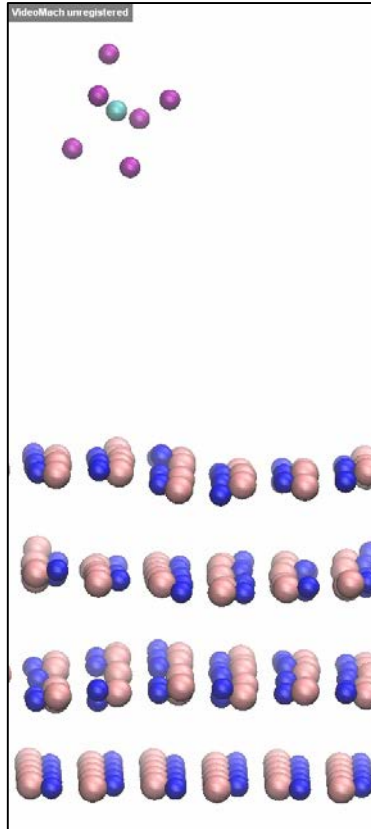
If someone ask about the low activation energy...

The activation energy is much lower than the bond energy, because F atom doesn't need to dissociate at very far site and... + other catalytic roles? (surface can make an activation energy lower ?)

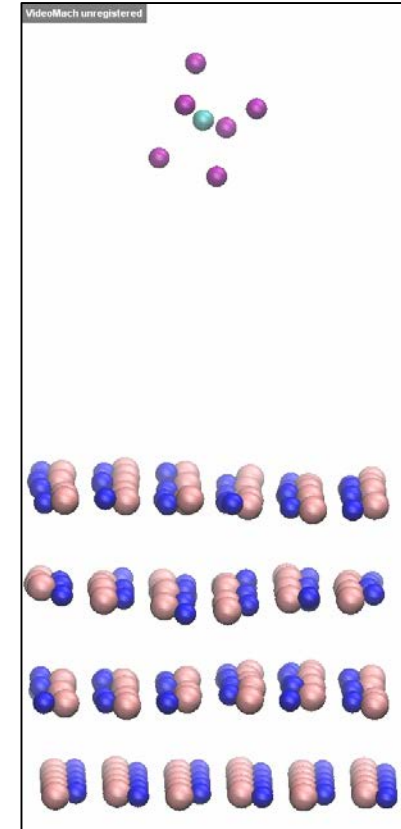


3. Kinetics, Transfer channels and Role of Phonons

- AIMD results show that the chemisorption reaction occurs over 500 K, and at 800 K adsorption does not occur*. It can be easily expected from the reaction kinetics that the dissociative sticking probability decreases exponentially as the substrate temperature is lowered, considering the low incident energy of the molecule [1]. So, our reported results are for 600 K and 200 m/s (most probable speed, MPS) from Maxwell-Boltzmann velocity distribution [2]. The **dissociation** occurs with this condition (Left). B and N heavy isotopes (1.2 times higher mass) also occur dissociation, but the reaction doesn't occur with B and N heavier isotopes (1.5 times higher mass) at same conditions (right).



Movie 2. AIMD result with normal B and N atoms.

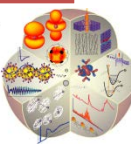


Movie 3. AIMD result with B and N heavier isotopes.

*We have not fully explored, but some combinations of high temperature and speed may react.

[1] R.D. Muino and H.F. Busnengo, Dynamics of Gas-Surface Interactions, (Springer-Verlag, Berlin, 2013).

[2] M. Kaviani, Heat Transfer Physics, 2nd ed. (Cambridge University Press, New York, 2014).



Target B-Atoms Transient Vibration Response

- **z-direction displacement-square** of B atom shows vibration characteristics after each events.

- As XeF_6 pulled toward the surface, z-direction displacement of B atoms becomes larger than that before event, and the adsorption occurs on the surface. The interaction of XeF_6 with surface is weak, so electron charge is small comparing to that of the chemisorption.
- Chemisorption occurs rapidly within 32 fs which is coincident to the simulation result in [1] that the time required for fluid particles approaching near surface to exchange energy with phonons is about 35 fs. The graph becomes denser after the reaction, which shows that vibration frequency is increased. Electron density shows that F/h-BN bond is formed as F and B atom attracting each other.
- As a product, XeF_4 is formed and starts desorbing after 400 fs from chemisorption. Interaction becomes very weak again as we can see from electron charge.
- h-BN thin film with B and N heavier isotopes cannot make reaction, and XeF_6 remains adsorbed on the surface. The vibration doesn't change significantly because there is no reaction.

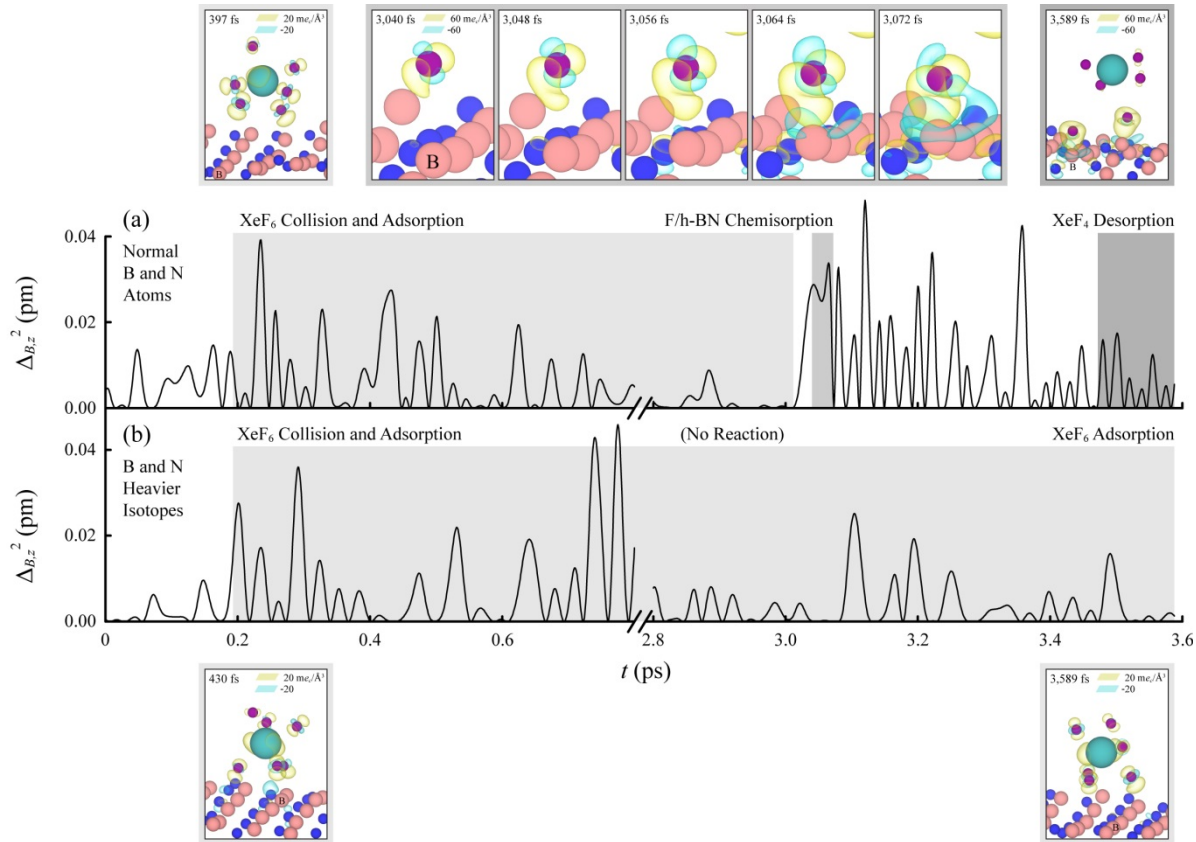


Fig. 12. z-direction displacement-square of B atom obtained by AIMD calculation with snapshots with distribution of electron density difference for (a) normal B and N atoms and (b) B and N heavier isotopes. Initial time is shifted to the point where XeF_6 is near the surface. Regions for each event from its starting are shaded with different gray scales. XeF_6 chemisorbed on the B atom of h-BN surface with normal atoms after adsorption, but h-BN with B and N heavier isotopes cannot make the reaction with the molecule.



Energy Transfer Channels

- Transient frequency analysis for the displacement of B atom

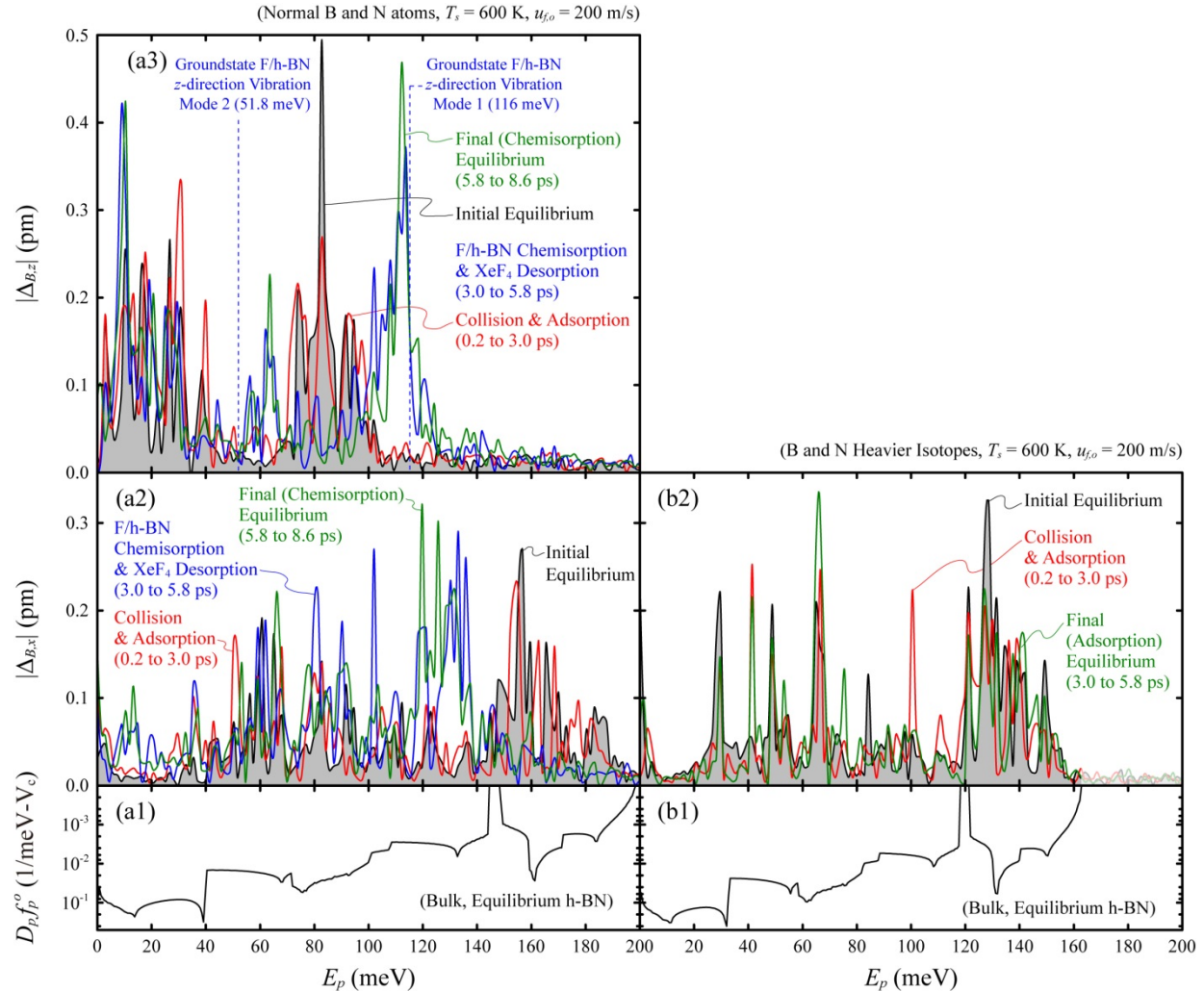


Fig. 13. Transient spectral analysis for displacement of B atom from AIMD result and comparison with phonon population for bulk h-BN at equilibrium for (a) normal h-BN and (b) B and N heavier isotopes. (1) Phonon population, (2) FFT for x direction, and (3) FFT for z direction with F/h-BN z -direction vibration modes. Data during 2800 time steps for each event was used to implement FFT, and time scale is same to that in Fig. 12. F/h-BN chemisorption occurred by normal B and N atoms change the distributions of phonon energies dramatically, but B and N heavier isotopes cannot trigger the reaction and phonon energy bands remain almost same. Note that phonon energies over 163 meV do not exist in B and N heavier isotopes physically, and this region shaded lightly in (b2) is due to the FFT limitation (Noise).



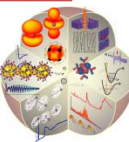
Phonocatalysis

- Using *ab initio* calculations we showed that heterogeneous (chemisorbed) reaction (dissociation) on large bandgap semiconductor surface can be controlled by its phonons. For h-BN, the three-phonon interaction time constant is about 0.57 ps and tracking the of instantaneous atomic displacement of surface-reaction atoms shows that reaction takes place in less than 0.1 ps. So the reduction in the phonon cutoff energy and resort to the multi-phonon absorption option prohibits the reaction.
- In addition to the isotope control shown here, phonons can be controlled by layered structures with the surface layer providing the surface-reaction-mediation effect and the subsurface layer mediating with the required-controlled phonons (with strong interlayer coupling).

[1] C. Hess, S. Funk, M. Bonn, D.N. Denzler, M. Wolf, and G. Ertl, Appl. Phys. A 71, 477-483 (2000).

[2] M. Beye et al., Phys. Rev. Lett. 110, 186101 (2013).

[3] M. Dell'Angela et al., Science 339, 1302-1305 (2013).

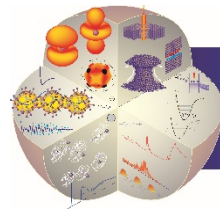


5. CONCLUSIONS AND OUTLOOK:

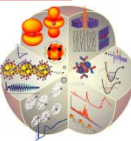
Through multiscale analyses we introduced and showed:

- The *phonon-recycling in graded heterobarrier* converts phonon energy back (partially reversing joule heating). We estimate up to 20% of the phonon energy conversion with proper electric current.
- We suggest optical phonon-bandgap *phonovoltaic* for recycling phonons and generating electricity. The search for effective pV material continue.
- We introduce *phonocatalysis*, aim and controlling surface reactions through substrate phonons.

Resonant-phonon harvesting can contribute to the future of our energy conversion and conservation.



Heat Transfer Physics



Acknowledgement

- The work is based on Ph.D. theses of Seungha Shin (now at University of Tennessee) and Corey Melnick (will graduate in Winter 2017), and Kwangnam Kim, and I am grateful to them for presenting their work.
- Research support by NSF (Thermal Transport and Processing) and DOE (Office of Basic Sciences).
- I am thankful to Professor Shigeo Maruyama for his hosting this seminar (and for his inspiring work), and Tokyo Tech for my visit as a World Class University invitation (my host, Professor Katsunori Hanamura).

